ABSTRACT

Title of Thesis:	HYDROGEL SELECTION AND CIRCUMFERENTIAL VASCULAR SMOOTH MUSCLE CELL ALIGNMENT FOR AN ARTERY-ON-A-CHIP
	Jesse Vo, Master of Science, 2020
Thesis Directed By:	Dr. Alisa Clyne, Department of Bioengineering

Atherosclerosis leads to cardiovascular disease, which is the greatest cause of the death in the US. Atherosclerosis begins with endothelial dysfunction, including reduced nitric oxide production and subsequent vascular smooth muscle cell relaxation. Current methods to measure endothelial dysfunction are complex, low-throughput, and often require tissue harvested from animals, which limits human translation.

Here, we present the foundation for a contractile artery-on-a-chip to investigate endothelial dysfunction. This device is comprised of a hydrogel channel in which human endothelial cells can be seeded together with circumferentially aligned vascular smooth muscle cells. In this thesis, I present data showing that the hydrogel channel can be made from a 1:1 collagen/GelMa blend and withstand 20μL/min flowrate. I also present a method to circumferentially align vascular smooth muscle cells inside a channel on feature sizes as large as 0.35mm. Together, these components bring us closer to realizing an *in vitro* artery-on-a-chip with contractile capability.

HYDROGEL SELECTION AND CIRCUMFERENTIAL VASCULAR SMOOTH
MUSCLE CELL ALIGNMENT FOR AN ARTERY-ON-A-CHIP

by

Jesse Vo

Thesis submitted to the Faculty of the Graduate School of the

University of Maryland, College Park, in partial fulfillment

of the requirements for the degree of

Master of Science

2020

Advisory Committee:
 Professor Alisa Clyne, Chair
 Professor Gregg Duncan
 Professor Helim Aranda-Espinoza

Contents

1. Introduction

1.1 Clinical Relevance: Cardiovascular Disease and Atherosclerosis

Cardiovascular disease (CVD) is the leading cause of death in the United States. The American Heart Association (AHA) reported in their 2020 Heart Disease Stroke Statistics update that more than 850,000 CVD-related deaths were recorded in 2017. CVD also has a profound financial impact. The same AHA report estimated that over $350 billion was spent on CVD from 2014 to 2015. This total includes both direct costs, such as hospital inpatient stays as well as emergency department visits, and indirect costs, such as lost productivity. These statistics are reflected globally, with CVD being the leading cause of death worldwide as well. CVD-related deaths are expected to reach over 20 million per year by 2030 [1].

CVD is an umbrella term for many conditions that affect the heart and/or blood vessels [2], most of which relate to atherosclerosis [3]. Atherosclerosis is characterized by lipid buildup in the arterial wall, eventually leading to atherosclerotic plaque formation [4]. The disease begins with endothelial dysfunction, which in turn enables lipids to permeate into the vessel wall. Leukocytes are also able to transmigrate through the disrupted endothelium. Some of these leukocytes differentiate into foam cells; lipid-laden macrophages that further plaque progression by producing proinflammatory cytokines [5]. In addition, smooth muscle cells proliferate and migrate into the atherosclerotic plaque. Indeed, vascular smooth muscle cells comprise the majority of foam cells [6]. In the latest stage, extracellular matrix (ECM) degradation destabilizes the plaque. As these plaques become increasingly unstable, they can eventually rupture, forming blood clots that completely occlude the vessel and leading to heart attack or stroke.

1.2 Arterial Structure and Function in Health and Disease

Arteries are made up of three tunica or layers: the outermost adventitia, consisting of connective tissue, blood vessels, and nerves; the middle tunica media, consisting of elastin fibers and smooth muscle cells; and the innermost tunica intima, consisting of a single layer of endothelial cells (ECs) attached to a basement membrane [7] as well as occasional vascular smooth muscle cells. Arterial structure differs depending on the local vessel requirements.

The three main types of arteries are elastic arteries, muscular arteries, and arterioles [8]. Elastic arteries, including the aorta, tend to be larger in diameter (>10mm) and have thick media layers. The larger vessel diameter and elastin-rich media layer allows these vessels to stretch in systole and snap back in diastole, reducing blood pulsatility. Conversely, muscular arteries, such as the femoral artery, tend to be smaller in diameter (10-0.1mm) and have relatively thinner media composed mostly of smooth muscle cells with little to no elastin fibers present [9]. These smooth muscle cells help muscular arteries vasoconstrict to control blood distribution throughout the body. Arterioles are small (<0.3mm) arteries that connect to capillaries. They are also known as resistance vessels for their role in resisting blood flow and thus decreasing blood pressure before the blood enters the capillaries. The capillaries are thin walled vessels, consisting of endothelium only, which allows efficient exchange of nutrients and waste between tissue and blood.

1.2.1 The Endothelium

The endothelium is the single layer of endothelial cells that line the vasculature. It serves many functions, such as wound healing and angiogenesis. It also maintains vascular tone, balancing vasodilation and vasoconstriction to regulate blood perfusion [10].

Endothelial vasodilation is driven in part by nitric oxide (NO) while vasoconstriction is driven by endothelin and vasoconstrictor prostanoids [11]. NO is of special importance, as dysfunctional NO production is an effective marker of overall endothelial dysfunction [12].

1.2.2 Normal Endothelial Cell Function: Shear Stress Response and NO Production

ECs form a continuous monolayer to line the entire vascular system, including arteries, capillaries, and veins [13]. As a result, these cells are in direct contact with blood and other molecules found in the bloodstream, as well as the vascular wall. This allows the endothelium to communicate hemodynamic changes into the surrounding tissue [14]. These hemodynamic changes, such as increased shear stress, cause endothelial cells to align and elongate in the flow direction and evoke cardioprotective responses such as NO production in the healthy endothelium. Endothelial cells sense shear stress through several different mechanosensors, including integrins, the glycocalyx [15], ion channels [16], intercellular junction proteins such as PECAM-1 [17], and even the actin cytoskeleton itself [18].

Endothelial NO production is a gold-standard measure of endothelial health. NO dilates blood vessels and protects the endothelium by inhibiting platelet and leukocyte adhesion [19]. NO also acts as an anti-inflammatory agent and antioxidant [20]. Endothelial nitric oxide synthase (eNOS) is the primary NO producing enzyme in the endothelium. The enzyme is dimeric and contains two domains which bind NADPH, flavin mononucleotide, flavin adenine dinucleotide, tetrahydrobiopterin (BH_4), oxygen, and L-arginine [21]. NADPH, molecular oxygen, and L-arginine are the primary substrates for NO production while the flavins and BH_4 serve as cofactors. One of the domains also contains a calmodulin binding sequence that, once bound, initiates the NO production process [22]. Electrons

from NADPH are passed between the eNOS domains to reduce molecular oxygen, which combines with L-arginine to ultimately produce NO and L-citrulline [21]. Despite its normal protective function in producing NO, eNOS may also contribute to CVD since it can produce reactive oxygen species in its uncoupled form [23].

1.2.3 Endothelial Dysfunction in Atherosclerosis

Endothelial dysfunction initiates atherosclerotic plaque formation [22, 23] and can be caused by several factors. Disturbed blood flow is well established to promote endothelial dysfunction and is supported by preferential atherosclerotic plaque formation at vessel bifurcations, where flow would be disturbed compared to straight vessel sections where flow is more unidirectional [26]. This disturbed flow is characterized by lower resulting shear stress on the endothelium and by areas of recirculation. Through mechanotransduction, reduced shear stress from disturbed flow activates proatherogenic effects in ECs. Many of these effects relate to the inverse of the atheroprotective EC effects previously mentioned. Proatherogenic ECs are proinflammatory, promote vasoconstriction, and produce reactive oxygen species [24]. As mentioned before, these ECs also have decreased NO bioavailability. These effects together promote atherosclerotic plaque development.

1.2.4 Vascular Smooth Muscle Cells

Vascular smooth muscle cells (SMCs) actively contract and relax to constrict and dilate the vessel, respectively. As with all smooth muscle cells, their activity is involuntarily and is instead controlled by regulating molecules in the bloodstream and produced by the neighboring ECs. NO is one such vasodilation regulating molecule. To successfully carry

out their function, SMCs assume a particular orientation. Specifically, they are circumferentially aligned about the vessel lumen, forming a ring-like structure [27].

1.2.5 Normal Function of SMCs: Contractile Machinery

SMC contraction can be initiated by mechanical, hormonal, or neural stimuli [28]. Regardless of stimulus type, the initiating contractile event is an influx of Ca^{2+} [29]. Ca^{2+} may come from outside the cell or from the Ca^{2+} stores in the sarcoplasmic reticulum. Ca^{2+} binds to calmodulin in a 4:1 ratio causing a conformational change in calmodulin. This conformational change allows myosin light chain kinase (MLCK) to also bind, forming a Ca^{2+}-calmodulin-MLCK complex which activates MLCK and phosphorylates one of the two light chains of myosin. Phosphorylated myosin forms cross bridges with cytoskeletal actin and produces the forces necessary in contraction.

SMC relaxation is initiated either indirectly by removal of the contractile stimuli or directly by a vasodilator, such as NO. Intracellular Ca^{2+} levels are decreased, either by complete removal from the cell or by Ca^{2+} sequestration in the sarcoplasmic reticulum [30]. Additionally, relaxation requires increased myosin light chain phosphatase (MLCP) activity, which returns myosin to its inactive state.

1.2.6 SMC Dysfunction in Atherosclerosis

Similar to ECs and the endothelium, SMCs also become dysfunctional in disease. In early atherosclerosis, specifically the pathological intima thickening stage, SMCs present decreased alpha smooth muscle actin (αSMA) expression. αSMA plays an integral role in contraction as described previously [31]. This is the first indication SMC phenotype switching away from the healthy contractile phenotype and towards the pathological proliferative/synthetic phenotype. SMCs in this stage of atherosclerosis also present

increased apoptosis [32] and expression of chemokines that recruit monocytes [33]. In later atherosclerosis, SMCs show more extensive phenotypic switching, resembling foam cells [34] and macrophages [35], which further progress the atherosclerotic disease state.

SMC phenotype change also occurs during cell culture, hindering *in vitro* SMC study. During cell culture, expression of contractile marker proteins, such as smooth muscle myosin heavy chain (MHC) and smoothelin, are decreased [36]. This may be caused in part by the traditional cell culture process in which cells are encouraged to proliferate by media supplemented with growth factors. Thus, a major challenge for *in vitro* SMC studies is maintaining or inducing contractile phenotype during cell culture.

1.3 Current Methods to Study Endothelial and Smooth Muscle Dysfunction

As described previously, endothelial dysfunction is an important marker of poor vascular health and an initiator of atherosclerosis. Therefore, methods to quantify endothelial dysfunction would be helpful in studying disease development and progression. Several methods are currently available to measure endothelial dysfunction.

1.3.1 NO Measurements

Measuring NO is arguably the most straightforward method of determining endothelial dysfunction but presents several challenges since NO is inherently unstable and has a short half-life [37]. Despite this challenge, NO has been measured in humans using a electrochemical microsensor [38]. However, these experiments suffered many issues including fragile equipment, which means that gathering large amounts of reproducible data in this fashion is not a feasible approach.

Current techniques for directly measuring NO still use electrochemical electrodes. Amperometry is class of techniques to measure relevant NO levels *in vitro* and *in vivo* [39]. In amperometry, a voltage is applied between two electrodes in steel sleeves. The sleeve tip is covered with an NO-selective membrane. NO from the sample diffuses through the membrane and is oxidized. The amount of oxidation is measured by the current between the two electrodes. More modern amperometric approaches use NO-scavenging membranes instead of NO-selective membranes, improving measurement specificity [40]. However, these electrochemical, electrode-based methods also have some disadvantages. As with most probe-based assays, the probe position can drastically affect results. Furthermore, at the picoamp measurement scale, electrical noise can muddy the acquired signal, even with Faraday-shielded probes. Indirect approaches of probing for NO

molecules have also been developed. These techniques measure either a byproduct of NO production or a resultant effect of NO bioavailability. For example, NO production can be estimated by measuring eNOS activity. Radioactively-labelled L-arginine is converted to L-citrulline by eNOS during NO production, which can be readily quantified [41]. Nitrate is another byproduct of NO and has also been used to indirectly measure NO [42]. However, this approach is less specific than the citrulline assay [43]. Finally, NO production can be measured via fluorescent probes such as DAF-FM diacetate, which permeates the cell membrane and fluoresces after reacting with NO [43].

1.3.2 Flow-mediated Vasodilation

Flow-mediated vasodilation (FMV) is an arterial response in which the vessel dilates as a result of increased blood flow [44]. This increase in blood flow increases shear stress, inducing NO production, thus leading to vasodilation. In FMV to study arterial function, B-mode ultrasound is used to visualize the diameter of a large surface vessel, often the brachial or femoral artery. The vessel diameter is then measured in three conditions: baseline, during hyperemia induced by a blood pressure cuff, and after stimulation of NO production enhancers such as bradykinin. This compares the endothelium at rest, during endothelium-dependent vasodilation, and during endothelium-independent vasodilation, respectively [45]. In these experiements, dilation by increased shear stress has been reported to be on the order of 10% compared to baseline [46].

FMV based assays are appealing as they are non-invasive and can be used with human subjects, but they offer very low throughput and require specialized training to perform and analyze. In addition, the reliance on ultrasound limits FMV based assays to larger surface vessels, precluding the study of resistance vessels.

1.3.3 Wire and Pressure Myography

Myography is a class of techniques to measure vessel function using harvested vessel samples [47]. In wire myography, resistance vessels are harvested, and two fine wires are threaded through the vessel. One wire is anchored to a micrometer while the other is anchored to a force transducer. As the vessel contracts and relaxes the transducer quantifies the force data [47].

Pressure myography is similar to wire myography with a slightly different setup. Instead of threading wires through the vessel, the sample is loaded onto two cannulae such that flow can be directed through the vessel. This vessel-cannula setup is kept inside a small chamber, similar to wire myography, but with the added functionality of allowing an outside flow to be run at the same time as the vessel flow. Both flows can be controlled, and the flow solutions can be treated and conditioned with molecules and proteins of interest. A camera is used to measure changes in vessel diameter, similarly to the methodology of FMV [48]. In pressure myography, high dosages of acetylcholine have been reported to constrict vessels up to 80% [49].

In both wire and pressure myography, a live vessel sample is required. Maintaining animal models is costly, and harvesting tissue samples poses ethical concerns. Harvesting and handling vessel samples also requires specialized training. Furthermore, results from animal models are not fully translatable to human physiology.

1.3.4 Vessel-on-a-chip Devices

Organ-on-a-chip systems are 3D *in vitro* cell culture platforms that recapitulate the *in vivo* cellular environment and stimuli [50]. This allows cells in culture to be significantly more representative compared to traditional 2D culture and circumvents the need for live

tissue harvesting. The organ-on-a-chip is specifically designed for the cells and organ of interest. In the case of vessel-on-a-chip devices, this involves designing a lumen-like channel structure on which ECs can be seeded and through which flow can be directed. This can be achieved through the use of sacrificial molds or soft lithography [51]. Other approaches circumvent the use of cells by harvesting vessel samples directly from animals [52]. Yasotharan *et al.* developed a microfluidic device in which small artery samples could be loaded and directly observed during vasodilation and vasoconstriction [53]. As convincing as these data are, this approach requires invasively harvesting tissue from animals. Thus this approach is not as relevant to human disease since human cells are not used and is throughput limited similarly to myography as harvested tissue samples are required.

Vessel-on-a-chip devices are advantageous in that they can be used to achieve results comparable to that of native vessels without the related costs of maintaining animals or waiting on sample donors. As they can be produced as needed, throughput is improved compared to other methods. Furthermore, human cells can be used, opening possibilities for personalized assays and pharmacological development. However, as with all previously described methods, vessel-on-a-chip devices also have inherent disadvantages. As they are manually fabricated, certain methodologies invite opportunities for variability among devices. This also increases the difficulty in reproducing these devices by peers. Despite these disadvantages, vessel-on-a-chip devices are powerful tools that can be customized for specialized test conditions.

Many current vessel-on-a-chip devices feature human ECs in their design. These ECs are sometimes seeded on substrates that are relatively rigid compared to the adventitia,

such as polydimethylsiloxane, while other approaches seed cells on hydrogels that are more mechanically and biologically representative of the native anatomy. However, as of yet, no vessel-on-a-chip device has been created with human ECs and SMCs integrated in such a way that the vessel can contract and relax to an appreciable, visually observable degree. The ability to vasoconstrict and vasorelax fundamentally distinguishes this artery-on-a-chip from prior vessel-on-a-chip devices.

1.4 Directed Cell Alignment In 2D and 3D

In vivo, ECs and SMCs are specifically aligned to facilitate their particular function. ECs are aligned in the blood flow direction [13], and SMCs are aligned circumferentially about the vessel (referred to as "3D alignment") [27]. Therefore, to create a representative vessel-on-a-chip device, these alignments must be recreated. In 2D (flat) systems, this has been accomplished through several means, including topographical features [54], electrical stimulation [55], and mechanical forces [56]. 3D cell alignment has been less studied but will be integral in the vessel-on-a-chip to be developed here.

1.4.1 Topographical Features

A common approach to directed, *in vitro* cell alignment is to seed them on surfaces that contain physical, micro- or nano-scale alignment features. This can be as simple as a micro-ridge pattern, which has been demonstrated to effectively align ECs [54]. Briefly, silicone groove and ridge features of various dimensions (400-4000nm pitch) were fabricated using x-ray lithography and used as master molds to pattern polydimethylsiloxane stamps. An optical adhesive that cures to a rigid polymer upon exposure to UV light was spin coated in tissue culture plates to form a flat layer. The PDMS stamps were pressed into this adhesive layer prior to UV exposure and then were removed. This formed ridged alignment patterns in the tissue culture plates. ECs seeded on these topographic patterns began to align in the direction of the grooves and ridges in as little as 30 minutes, with longer adherence time increasing the degree of alignment.

SMCs have also been aligned using topographical methods [57]. Instead of a flat, patterned surface, SMCs were seeded on synthetic elastin (SE) fibers aligned by

electrospinning. Compared to cells seeded on a glass control group and cells seeded on randomly arranged SE fibers, SMCs seeded on the aligned SE fibers were greatly aligned.

1.4.2 Electrical Stimulation

Electrical fields have also been demonstrated to effectively align ECs [55]. Both the electrical field intensity as well as the exposure duration affect EC alignment. Higher voltages (>75mV/mm) and longer durations (>4 hours) tend to align cells to a greater degree. Electrical stimulation is known to induce vascular endothelial growth factor receptor (VEGFR) activation [58], and so VEGFR was hypothesized as the mechanism underlying EC reorientation. This hypothesis was confirmed by increased VEGFR levels in the cell culture media of electrically stimulated cells compared to unstimulated cells. Also, chemical inhibition of VEGFR resulted in total loss of cell alignment behavior even under electrical stimulation [55]. This hypothesis was further explored, and it was discovered that downstream of VEGFR activation, phosphatidylinositol-3-kinase (PI3K)-Akt and Rho-ROCK activation are major pathways that result in EC reorientation.

1.4.3 Mechanical Forces

Mechanical forces can also be applied to align cells *in vitro*. As described previously, ECs align when subject to physiological shear stress and can be aligned *in vitro* using this approach. A parallel plate flow chamber was specifically designed to allow concurrent traction microscopy to elucidate this cellular response [59]. Briefly, it was discovered that the initial response to shear stress from laminar flow is a rapid decrease in intercellular stresses which is followed by slower alignment of the EC body. While these types of stimuli are naturally present, their application to SMCs is not as relevant as their application to ECs. In addition, engineering these types of forces consistently *in vitro* poses

a greater technical challenge than consistently creating alignment features for topographical alignment.

1.4.4 Cell Alignment Methods in 3D

While aligning cells in 2D, that is, on a flat surface, has been well documented with various approaches, directing cell alignment in 3D is a significantly greater challenge. Many approaches are related to tissue engineering practices involving scaffold fabrication [60]. For example, SMCs alignment in 3D was achieved using a novel layer-by-layer seeding method. Briefly, a thin (60 µm) film microchannel scaffold was fabricated using a topographically patterned polydimethylsiloxane mold in a process similar to the EC topographical alignment method described previously. SMCs were seeded onto this scaffold and maintained until confluent and aligned. A that point, a thin hydrogel layer was deposited on the cell monolayer. A second thin film microchannel scaffold was fabricated on top of this hydrogel layer, and a new cell layer was seeded as before. This process was repeated until a 3D structure of aligned SMCs was achieved. In theory, the microchannel structure could be modified to create different alignment patterns, but this has not yet been explored. While this approach is straightforward and does indeed achieve 3D alignment of cells, an extended time period is required for each cell layer to adhere and reach confluency.

1.5 Thesis Overview

In this thesis, several important steps were taken in the process of creating an artery-on-a-chip for pressure myography using human ECs and SMCs. Specifically, a more stable channel was created in a collagen - gelatin-methacryloyl (GelMa) blend hydrogel to enable longer term culture of the artery-on-a-chip; and second, a new technique was developed to circumferentially align SMCs inside the channel.

Aim 1: Collagen/GelMa Channel Formation & Endothelial Cell Adhesion

Prior attempts to create a channel within a collagen hydrogel for the artery-on-a-chip were unreliable and unstable. We therefore decided to use a collagen/GelMa blend for the hydrogel channel. Different concentrations of collagen, GelMa, and photoinitiator were tested to determine which combination would create a stable channel on which ECs could be seeded to form a vessel lumen-like structure.

Aim 2: Topographical Circumferential Alignment of Vascular Smooth Muscle Cells

Although quite effective and straightforward in 2D, topographical alignment can be difficult in 3D. We therefore developed a novel technique in which the ridges created during 3D printing are used to create topographical features in the collagen/GelMa hydrogel. We tested the technique on flat surfaces, curved surfaces, and inside a channel.

2. Collagen/GelMa Hydrogel Channel Formation & Endothelial Cell Adhesion

2.1 Introduction

Hydrophilic gels, more commonly referred to as "hydrogels," are large 3D polymer networks of crosslinked hydrophilic chains [61]. In practice, hydrogels can be formed through a variety of methods. Some involve neutralization of the dissolved polymer solution which induces auto-assembly. Others require crosslinking neutral polymers dissolved in water with a crosslinking agent activated by an external energy source such as ultraviolet (UV) light [62]. Regardless of the polymerization method, the tunable, hydrophilic, and biocompatible nature of hydrogels make them a favorable biomaterial for biomedical research. As such, hydrogels are used in many different areas of biomedical research, including tissue engineering [63], drug delivery [64], and even wound healing [65]. In this chapter, we use channels formed in collagen- and gelatin-based hydrogels as the foundation for the artery-on-a-chip device.

Our hydrogel channel fabrication process is based on a design created by Peter Galie [66]. Briefly, Galie's design consists of a chamber formed between two polydimethylsiloxane (PDMS) slabs. The chamber is then filled with a prepared collagen solution. Two thin needles are inserted into the chamber, after which the collagen solution is exposed to the proper temperature (37°) to form a hydrogel. The needles are then removed, resulting in two parallel micro-channels. These channels are then seeded with cells and subjected to flow. In our experiments, this method sometimes produced a viable channel, but more often than not the channel collapsed either prior to or after the application of flow. This was due to several factors. First the channel diameter in Galie's design was significantly smaller than the channel diameter required for our purposes. In addition, the

gel composition in Galie's design could withstand flow to their specifications (2.4μL/min) but could not maintain structural integrity at higher flow rates. Thus, a new hydrogel was needed to increase channel stability.

I modified the gel composition by adding a gelatin methacryloyl (GelMa) component to create a more stable hydrogel for cell seeding and flow experiments. GelMa is a UV crosslinkable hydrogel composed of gelatin and methacrylic anhydride. Gelatin is hydrophilic polymer produced by hydrolizing collagen [67]. Methacrylic anhydride is a liquid that when reacted with certain organic compounds leads to the attachment of methacryloyl side groups, hence the name "gelatin methacryloyl." When dissolved in water and in the presence of a photoinitiator, GelMa can be readily crosslinked with exposure to UV light [68]. The main benefit of GelMa is its improved mechanical stability and adherence to PDMS compared to collagen hydrogels. Outside of organ-on-a-chip systems, GelMa has also been used to encapsulate cells [69], as scaffolds for load-bearing tissue [70], and as a delivery vehicle for bioactive molecules [67].

2.2 Methods

2.2.1 PDMS Device Fabrication

Device fabrication began with polymerization of a PDMS top. The PDMS was prepared with a standard 10:1 ratio of elastomer base and curing agent, respectively, which was thoroughly mixed by hand with a tongue depressor. 11g of PDMS prepared in this way was then poured into the lid of a 100 mm culture dish. The PDMS was degassed using a desiccator for at least 30 minutes to remove air bubbles created during the mixing. After the PDMS was free of air bubbles, the culture dish lid was placed in an 80°C oven overnight to complete the curing process.

Once the PDMS top was completely cured, a second batch of PDMS was prepared and degassed as above. A thin layer of wet PDMS was poured on top of the cured PDMS top in the culture dish lid. Then, the remaining wet PDMS was poured over eight previously fabricated positive molds of the final device design. The PDMS coated molds were then inverted onto the wet PDMS in the culture dish lid, and the PDMS was degassed again to remove any remaining air bubbles. This PDMS layer is hereafter referred to as the "device" layer. After 30 minutes of degassing, any air bubbles that remained were removed by hand using sharp-pointed forceps. At this point the culture dish lid was again placed in the 80°C oven for at least 20 but not longer than 30 minutes.

Once the device layer had solidified, the culture dish lid was removed from the oven. The entire PDMS top and device layers, which were now fused, was removed from the lid. The molds were carefully removed from the PDMS, leaving an open chamber and inlet ports. The PDMS was cut into eight individual devices and all devices were plasma treated (Harrick, PDC-001) along with eight 20x40mm rectangular coverslips (VWR, 48382-126)

on high for 1 minute. The inlet ports were then created with a 1mm biopsy punch (Miltex, 33-31AA-P/25).

A PDMS base was prepared in a 100 mm culture dish lid as described for the first slab. This base was cured until just barely solid, which occurred after approximately eight minutes in the 80°C oven. The eight separate PDMS device layers were inverted onto the PDMS base. The eight PDMS device layers were then cured with the PDMS base in the 80°C oven for at least 30 more minutes. The devices were then cut into eight individual, complete PDMS microfluidic devices. Each device was placed onto a coverslip and all devices were kept in the 80°C oven overnight to complete the curing process (Figure 2.1).
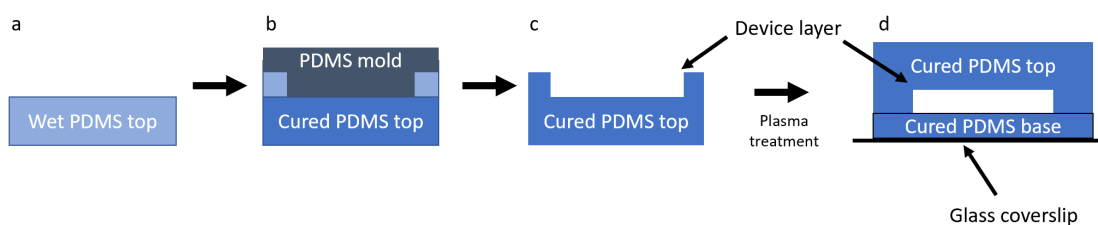
Figure 2.1: PDMS molding process for forming microfluidic device. (a) Wet PDMS was cured in a cell culture dish lid to form the PDMS top. (b) The PDMS molds were inverted onto a layer of wet PDMS on the cured PDMS top. (c) The PDMS molds were removed, leaving an open-faced device layer. (d) After plasma treating the device layer and glass coverslip, the cured PDMS top was bonded to a freshly cured PDMS base.

2.2.2 Collagen Hydrogel Gelation

PDMS devices were first coated with a thin layer of collagen to improve hydrogel attachment to the PDMS device and maintain structural integrity during flow. To prevent the uptake of small molecules [71], each device was treated with 200 µL of 5 M sulfuric acid for 90 minutes. The devices were washed 10 times with 1X phosphate-buffered saline (PBS, Gibco) prior to loading 10-50µg/mL Type-1 rat-tail collagen solution Gibco, A1048301), which was enough to fill the entire central chamber but not the inlet ports. The devices were then placed in a 37°C cell incubator for 1 to 3 hours to allow the collagen to adhere to the PDMS. After the collagen coating, the devices were again washed with PBS and kept in a 4°C refrigerator until use.

The collagen hydrogel solution was then prepared. All steps were performed in a biosafety cabinet to maintain sterility. Prior to beginning, deionized (DI) water, 10X PBS, 1M NaOH, 2 mL centrifuge tubes and collagen solution (either manually dissolved in acetic acid from a lyophilized solid (MP Biomedical, 150026) or pre-dissolved (Advanced Biomatrix, 5226) was placed on ice for 30 minutes to prevent premature collagen gelation during the hydrogel fabrication process. Then, 100 µL 10X PBS, 90 µL DI water, and 10 µL 1M NaOH were sequentially added to a 2 mL centrifuge tube and thoroughly vortexed. After mixing, 800 µL of collagen solution was added to the centrifuge tube to create an approximate final volume of 1000 µL. Solution pH was tested by pipetting a small volume of collagen solution onto a pH strip. 0.1 M NaOH was used to adjust the solution pH to 7.

Once the gel solution was prepared, the PDMS devices were retrieved from the refrigerator and kept on ice along with the gel solution. Needles ranging in diameter from 100 μm to 600 μm were dipped in 1X PBS and then inserted through the devices as shown in Figure 2.2. Up to 200μL of gel solution was injected into the device using a corner inlet port, and the devices were incubated again at 37°C for 1 to 24 hours to complete collagen gelation. If cells were not immediately seeded after gelation, devices were stored in a 4°C refrigerator until cell seeding.
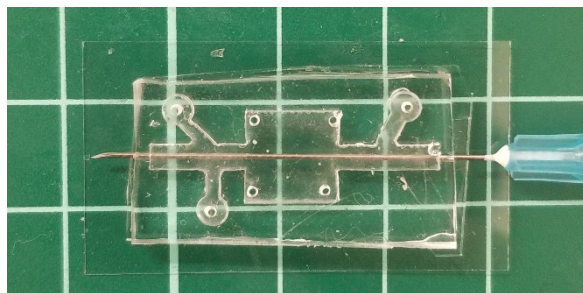

Figure 2.2: PDMS device with 0.5 mm diameter needle inserted prior to gel solution loading. Grid = 10mm.

The needle diameter ultimately determines the channel diameter. Resistance vessels in the body fall under 400μm diameters [72] which can be achieved by using smaller needles.

2.2.3 Gelatin Methacryloyl (GelMa) Synthesis

Gelatin methacryloyl (GelMa) was synthesized as an alternative to collagen hydrogels. Gelatin was first reacted with methacryloyl over 1 to 2 hours by dropwise addition of methacrylic anhydride (MA, Sigma Aldrich 276685) to Type A gelatin (G2500-500G, Sigma Aldrich). For 30 mL of 10% w/v gelatin in PBS, 2.3 mL of MA was added via syringe pump (New Era Pump Systems Inc., NE-1000) set at a flow rate of 20 μL/min. Solution temperature was maintained between 45°C and 50°C to prevent gelatin denaturation. The solution was vigorously stirred with a magnetic stir bar at 1200 rpm.

After the MA was fully added to the gelatin solution, the solution was transferred to a 50 mL Falcon tube and centrifuged at 1000g for 2 minutes to pellet the unreacted MA. The supernatant was then collected and diluted 1:1 with PBS to create a 5% w/v gelatin solution.

This solution was then dialyzed in two 10kDa MW cutoff dialysis cassettes (Thermo Scientific 66830) submerged in DI water in a 50°C oven for two days to remove any unreacted MA. DI water was refreshed each day.

The GelMa solution was then adjusted to pH 7-7.4 using 1 M NaOH. 35 mL of solution was then transferred to 50 mL Falcon tubes and frozen at -20°C for at least 30 minutes before further freezing at -80°C overnight. Once the solutions were completely frozen, all samples were lyophilized (Labconco, 700611000) for 5 days. The cotton-like white solid was stored in the dark at room temperature prior to use.

2.2.4 GelMa Devices

To create GelMa hydrogels within the previously described PDMS devices, solid GelMa was transferred into scintillation vials (Kimble, 74504-20) and UV sterilized for at least 30 minutes before dissolving in PBS for at least 30 more minutes at 37°C. Immediately before loading the GelMa solution, 20-60 µL of 5% lithium phenyl-2,4,6-trimethylbenzoylphosphinate (LAP) photoinitiator solution (Sigma Aldrich, 900889-1G) was added into the GelMa solution, and the scintillation vial was thoroughly mixed with a micropipette. Up to 200 µL of the GelMa-LAP solution was injected into each PDMS chamber prepared with needles as described previously. Several devices were collected into a 100 mm culture dish. The dish was sealed with Parafilm to prevent oxygen from inhibiting the crosslinking reaction. The GelMa was crosslinked with UV light (254 nm, Analytik Jena, 95-0230-01) for 3 to 10 minutes. The result was a solid, semi-translucent hydrogel inside the PDMS device. Devices were stored at 4°C until cell seeding.

2.2.5 Collagen/GelMa Blend Devices

In the final version of the device, a blend of collagen and GelMa was used for the hydrogel. The GelMa was synthesized and prepared as described previously. While the GelMa was dissolving in the incubator, a collagen solution was prepared as described previously. Immediately after adding the LAP photoinitiator to the GelMa solution, the GelMa solution and collagen solution were combined in various ratios and mixed thoroughly prior to loading into the PDMS devices. The solutions were first gelled by UV crosslinking as described in the GelMa devices section and then incubated at 37°C for up to 24 hours. The devices were then kept at 4°C until cell seeding.

2.2.6 HUVEC Culture

Human umbilical vein endothelial cells (HUVECs, Lonza, C2519A) were cultured in 100mm polystyrene dishes maintained with Endothelial Growth Media (EGM-2, Lonza, CC-4176). Media was replaced every other day, and cells were used between passages 3 and 8. In some experiments, GFP-mitochondria labeled cells were used. Prior to each experiment, HUVEC were washed with sterile PBS and detached from the culture dish with 2 mL of trypsin-EDTA (Gibco, 25200056). Cells were collected and counted using a Countess automated cell counter (Thermo Fisher Scientific, AMQAX1000). Cells were then concentrated by centrifugation at 5000RPM for 5 minutes, followed by removal of the appropriate volume of media to reach a cell density of approximately 5M cells/mL. Cells were resuspended by mixing.

During cell preparation, hydrogel-filled PDMS devices were kept at room temperature in the biosafety cabinet for at least 10 minutes. The needles were carefully twisted to separate them from the hydrogel and pulled out of the devices using forceps. Each channel was then loaded with 100 µL of EGM-2 and incubated at 37°C for at least one hour. 100µL

of the HUVEC solution was then loaded into each device such that approximately 500,000 cells were loaded into the channel. Devices were returned to the incubator for at least 30 minutes to allow cells to adhere to the channel. During that time, a second HUVEC suspension was prepared. 100 μL of the second HUVEC suspension was added to the channel, but the devices were inverted such that the second set of cells adhered to the opposite side of the channel. After 30 minutes, devices were returned to their initial orientation and covered with cell media. Devices were stored in the incubator for 24 hours to allow cells to spread in the channels.

2.2.7 Subjecting Cells to Flow

HUVECs within the channels were then subject to flow to induce alignment. Cell-seeded devices were transferred to a new 100 mm polystyrene dish with holes created in the lid using a soldering iron. Sterile 30 mL Luer lock syringes (BD, 309650) were filled with EGM-2 and assembled into a syringe pump (New Era Pump Systems Inc., NE-1600). Tygon tubing with 0.05 inch inner diameter (Component Supply, TND80-050) was used to connect to syringes to the device inlet ports. The flow rate was set between 5 μL/min and 340 μL/min. Cells were exposed to flow for 24 to 48 hours in a 37°C incubator.

2.2.8 Cell Fixation and Imaging

To image cells within the hydrogel channels, the channels were washed with cold PBS and fixed with 4% paraformaldehyde (PFA, Invitrogen, FB002) for 15 minutes on ice. All solutions were loaded into the hydrogel channels using a micropipette and gel-loading tips. The channels were washed again with PBS for 5 minutes. 0.1% Triton X-100 (Alfa Aesar, A16046-AP) was used to permeabilize cells for 5 minutes, followed by two additional PBS washes for 5 minutes each. Cells were blocked with 1% bovine serum albumin (BSA,

Sigma Aldrich, A9418) for 30 minutes and then labeled with 0.05% Hoechst (Invitrogen, H3570) and 1.25% rhodamine phalloidin (Biotium, 00027) for nuclei and actin, respectively. A confocal laser scanning microscope (Nikon, Eclipse Ti2-E) was used to image the hydrogel channels. Images were obtained at 10x and 20x magnification using 2.5 µm steps over a range of at least 500 µm to visualize the entire channel.

2.3 Results

2.3.1 PDMS Device

The first step in creating the hydrogel device was improving the method for air bubble removal from the PDMS devices. Initially, air bubbles were removed with degassing in a desiccator only. Devices created using this technique had large amounts of air bubbles (Figure 2.3). While primarily a cosmetic issue, these bubbles prevented effective observation of the gelation process and in some devices, appeared to hinder gelation as well. Manually removing air bubbles using sharp forceps reduced the air bubbles; however, some small air bubbles still formed during the 20-30 minute cure (Figure 2.4). Increasing degassing time to a minimum of 30 minutes removed the remaining air trapped in the wet PDMS, preventing air bubbles from forming in the PDMS during the curing process. These changes resulted in PDMS devices with few to no air bubbles for improved structural integrity and hydrogel visualization (Figure 2.5).
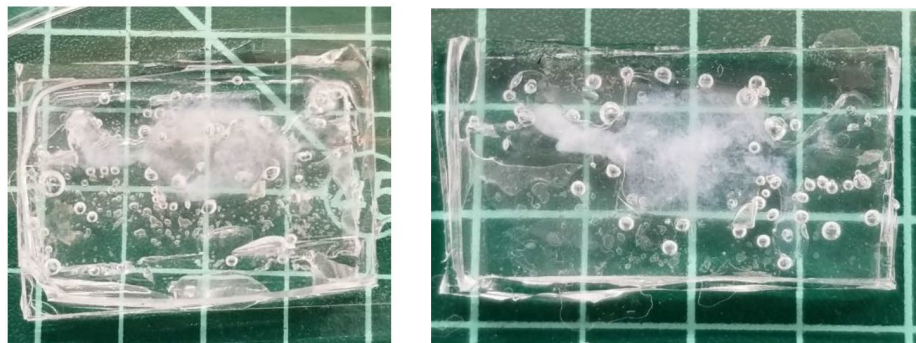
Figure 2.3: Initial PDMS devices created with only degassing and no manual bubble removal had large air bubbles that obscured viewing the channel and may have hindered hydrogel gelation. Grid = 10 mm.
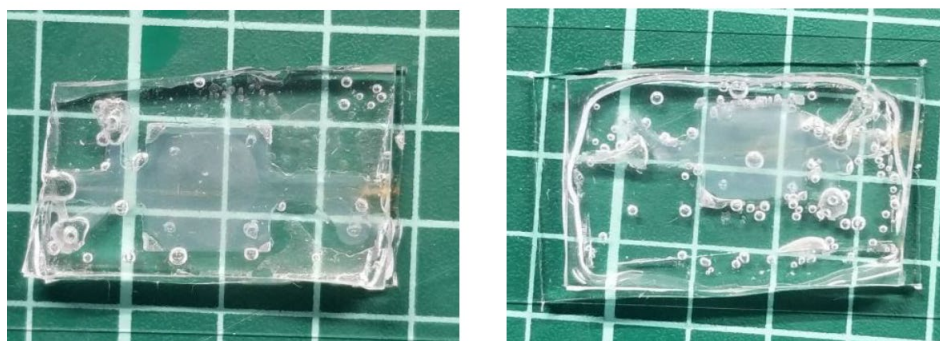
Figure 2.4: Manually removing air bubbles using sharp forceps reduced the number of air bubbles; however, additional bubbles still formed during the curing process. Grid = 10 mm.
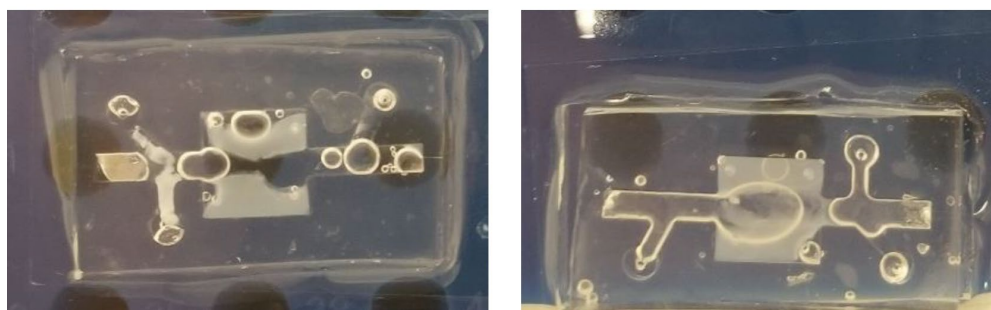
Figure 2.5: 30 minutes of degassing along with manual air bubble removal resulted in final PDMS devices with few air bubbles.

2.3.2 Collagen Hydrogel Gelation

The next step in creating the hydrogel device was improving the collagen gel. Initially, the collagen solution was manually prepared by dissolving lyophilized bovine collagen in acetic acid at room temperature over a 24-hour period. When collagen solutions prepared in this way were used, the collagen did not gel in most experiments (Figure 2.6). Even when the collagen did gel, needle extraction often disturbed the gel completely with no evidence of channel formation.

In these initial experiments, pH was measured using a pH meter (Fisher Scientific, AE150) equipped with a microprobe that fit inside a centrifuge tube. While the pH measurements acquired with this probe were more accurate and precise compared to those obtained with pH strips, the extended measurement time combined with the need to take several measurements led to premature collagen gelation. Using pH strips improved collagen gelation greatly by decreasing the time required to measure pH. Decreased measurement accuracy and precision was not a significant loss, as an approximate pH (~7.4) was sufficient for gelation.

I therefore formed the next set of hydrogels by dissolving collagen at 4°C and measuring pH with pH strips. This protocol resulted in more stable gels; however, gel formation remained inconsistent. Deionized water colored with orange dye was used to visualize collagen channels. As in previous samples, many gels were still disturbed upon needle extraction (Figure 2.7).

Final collagen devices were fabricated using commercially-available pre-dissolved collagen solution instead of manually dissolved collagen. While manually dissolving collagen is advantageous in that the collagen concentration can be controlled, it requires

careful pH titration which leads to variations in the final collagen concentration. Commercially-available pre-dissolved collagen facilitated more consistent pH and concentration control. Finally, rigid syringe needles instead of flexible acupuncture needles resulted in more stable channel formation, as the needle did not flex into the gel during removal (Figure 2.8).

Although collagen devices fabricated using the improved protocols were more stable and reliable in forming channels, the collagen gels were still not consistently stable and often were disrupted during flow. I therefore explored GelMa hydrogels due to the simple gelation process and the ability to control hydrogel mechanical properties in different ways: by adjusting the gelatin concentration, photoinitiator concentration, or UV crosslinking time. For these devices, 5% w/v gelatin and 0.1% w/v photoinitiator was UV crosslinked for three minutes. Compared to collagen devices, GelMa devices displayed more consistent gel and channel stability. In addition, the resulting gel was almost completely transparent (Figure 2.9).
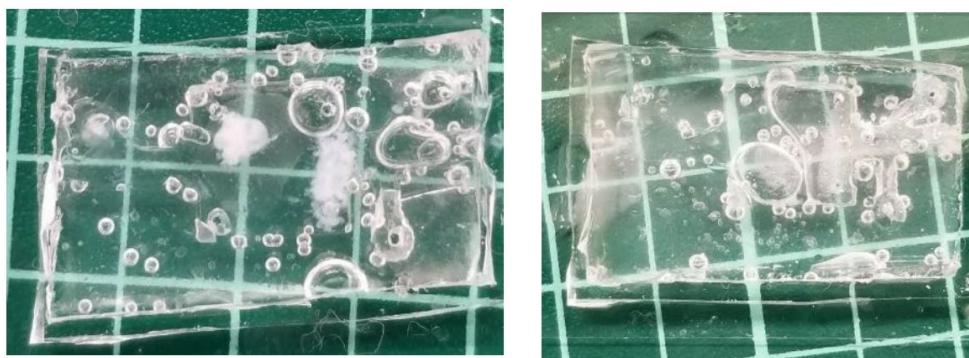
Figure 2.6: Lyophilized bovine collagen dissolved in acetic acid at room temperature for 24 hours did not gel within the device. Partially gelled collagen appeared cloudy white. Grid = 10mm.
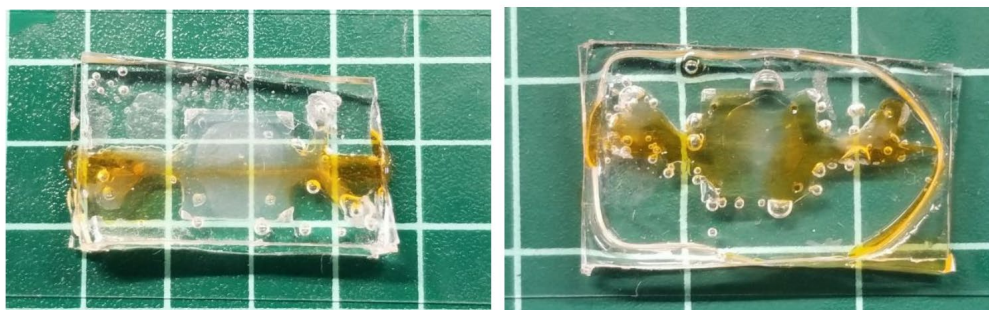
Figure 2.7: Collagen gels often became unstable within PDMS devices, as demonstrated using an orange dye to visualize the channels. Improved collagen procedures resulted in more stable gels (left), although many gels were still disturbed when needles were removed (right). Lyophilized collagen was dissolved at 4°C, and pH was measured with pH strips. Grid = 10mm
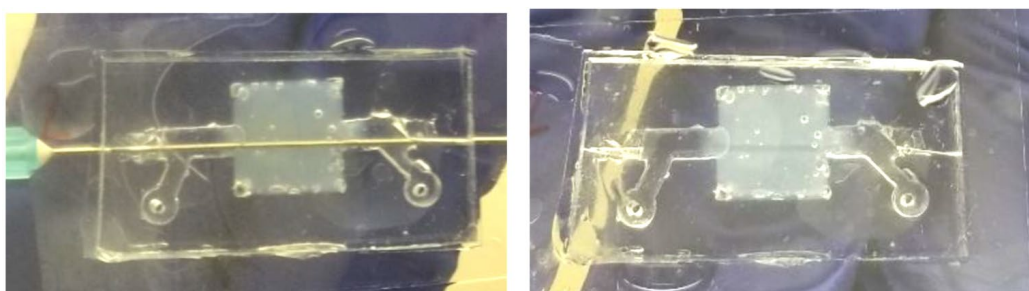

Figure 2.8: Gels fabricated with pre-dissolved collagen gel instead of lyophilized collagen resulted in more stable gels, especially after needle removal.
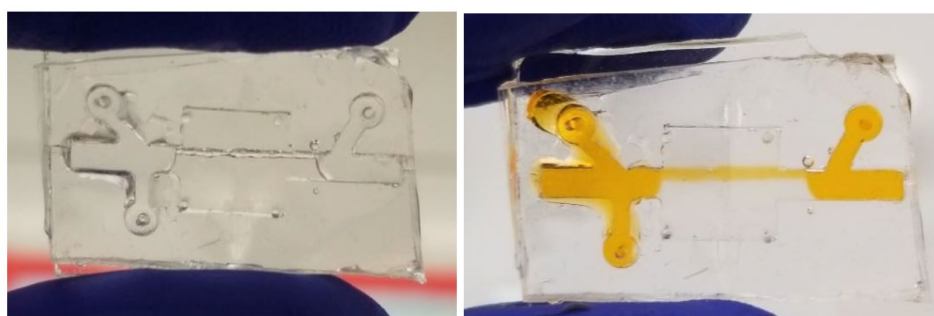

Figure 2.9: GelMa hydrogel devices were significantly more stable compared to collagen hydrogel devices and were more transparent. An orange dye was perfused through the GelMa channel with little resistance and no visible gel disruption.

2.3.3 Collagen/GelMa Blend Devices

While the GelMa devices were stable, they formed jagged edges inside the channels during needle removal likely due to gel binding to the needle during UV crosslinking. These edges did not prevent cells from adhering to the channel but might have disturbed flow and prevented endothelial cell alignment in the flow direction. To create a stable gel with a smooth channel, a blend of collagen and GelMa was explored. Various ratios of collagen to GelMa were tested . The 1:1 collagen/GelMa blend created a stable gel with a smooth channel. When collagen was increased, the gels became less stable without a discernable a change in channel smoothness (Figure 2.10). I therefore decided to use a 1:1 collagen/GelMa solution for the final hydrogel device.
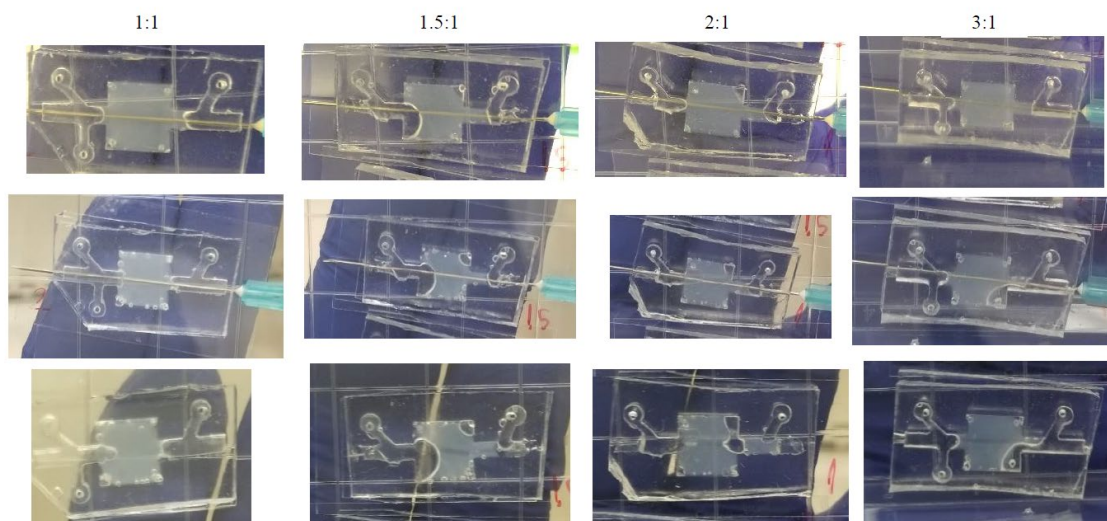

Figure 2.10: A 1:1 collagen/GelMa blend created a stable gel with a smooth channel. Collagen/GelMa blend devices made using different collagen GelMa ratios. (Top row) Gels prior to UV exposure. (Middle row) Gels immediately after UV exposure. (Bottom row) Gels after 37°C incubation and needle removal.

2.3.4 HUVEC Seeding

During development of each device type (collagen, GelMa, and collagen/GelMa blend), HUVECs were seeded into the devices when the channels appeared stable enough to support cell adherence. This seeding process also was improved over the course of the device development.

In collagen gels formed using manually dissolved collagen at room temperature, GFP-mitochondria labeled HUVECs were used to enable imaging immediately after cell seeding (Figure 2.11). In this way, I could ensure proper cell loading in the device and avoid damaging the unstable collagen gels by injecting cell fixation and labeling solutions. In these collagen gels, cells adhered to the collagen gel but did not exhibit expected spreading.

Collagen devices fabricated with manually dissolved collagen at 4°C and pH balanced with pH strips were seeded with unlabeled cells, which were then fixed and labeled for nuclei and actin as described previously. Cells in these devices demonstrated expected spreading, but in many devices, the gel was still not mechanically stable and a lumen-like ring structure was not formed (Figure 2.12). In some experiments with these devices, the cell seeding process disrupted the collagen gels. This did not affect the adherence and spreading of cells, but in these cases, the cells adhered to the PDMS device rather than the collagen gel.

When the pre-dissolved collagen solution was used, the first lumen-like ring structures were observed (Figure 2.13). Due to the large channel diameter, a lower magnification objective with a greater working distance was required to capture the entire channel. This resulted in lower confocal image quality, but enabled visualization of the clearly defined lumen-like ring structure when the z-stack was compressed as a maximum intensity

projection (MIP). However, the structure itself was not perfectly round. These imaging issues could be addressed by decreasing the working distance between the hydrogel channel and the microscope objective. Attempts were made to remove the bottom PDMS layer prior to imaging, but doing so caused significant damage to the hydrogel which had attached to the PDMS layer.

Initial GelMa devices resulted in more rounded channels (Figure 2.14). These GelMa devices were also the first instance of an observable channel that ran the entire length of the device. Previous devices at most had short stretches of observable channels that were interrupted by a disturbance or failure in the gel. However, the previously described jagged edges formed during needle removal had a significant effect on cell adherence and orientation.

1:1 collagen/GelMa blend devices also maintained a channel structure through the entire length of the device. With this specific gel formulation, smoother channel walls were observed compared to GelMa devices, but some major jagged features remained (Figure 2.15).
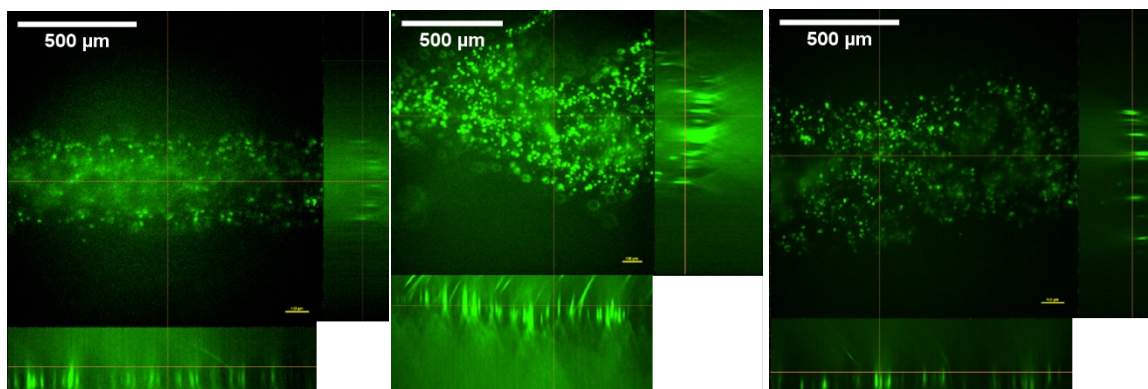
Figure 2.11: GFP-mitochondria labeled HUVECs adhered in the collagen channel but did not fully spread. Collagen solution manually dissolved at room temperature. Confocal microscopy, 10x magnification, scale bar = 500 μm.
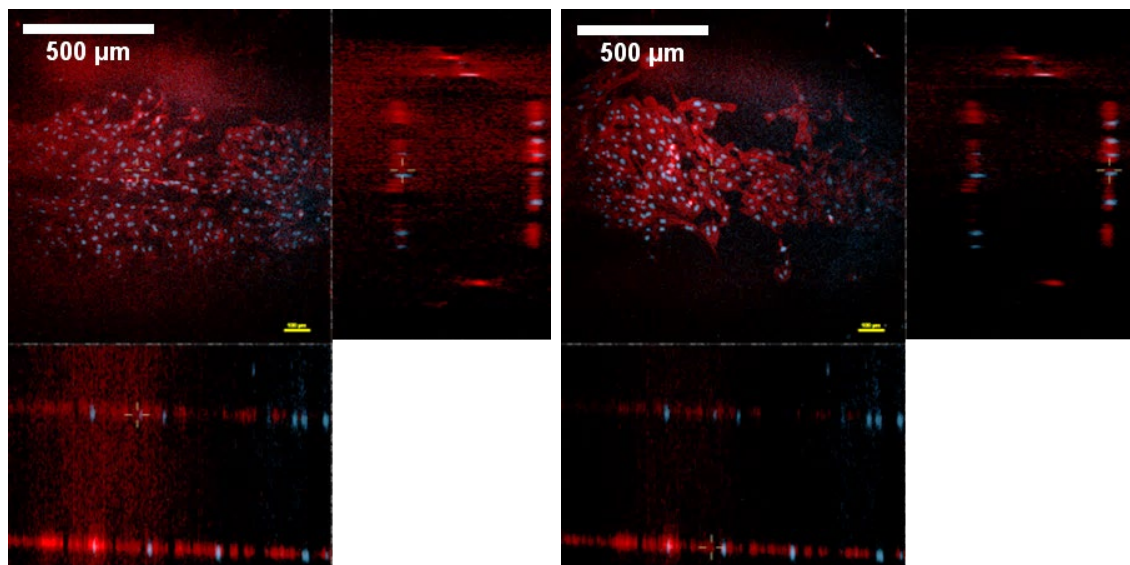
Figure 2.12: HUVECs seeded in channels made from lyophilized collagen showed signs of spreading, but the overall channel structure was not present. The collagen solution was manually dissolved at 4°C. Cells were fixed with paraformaldehyde and labeled for nuclei (blue) and actin (red). Confocal microscopy, 10x magnification, scale bar = 500 µm.

Figure 2.13: HUVECs seeded in collagen channel stained for actin and nuclei. Hydrogel formed using pre-dissolved collagen solution. Ring-like channel structure is present, but not round. Confocal microscopy, 10x magnification, scale bar = 500 µm.

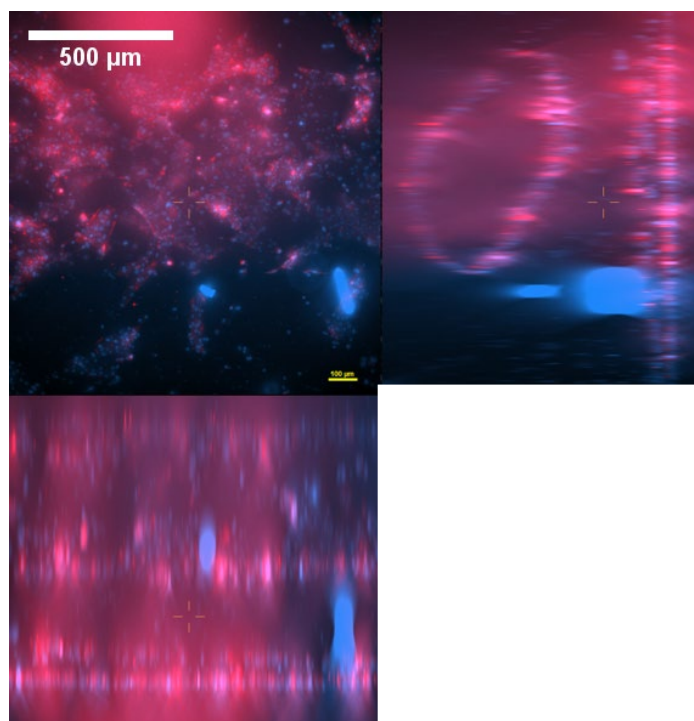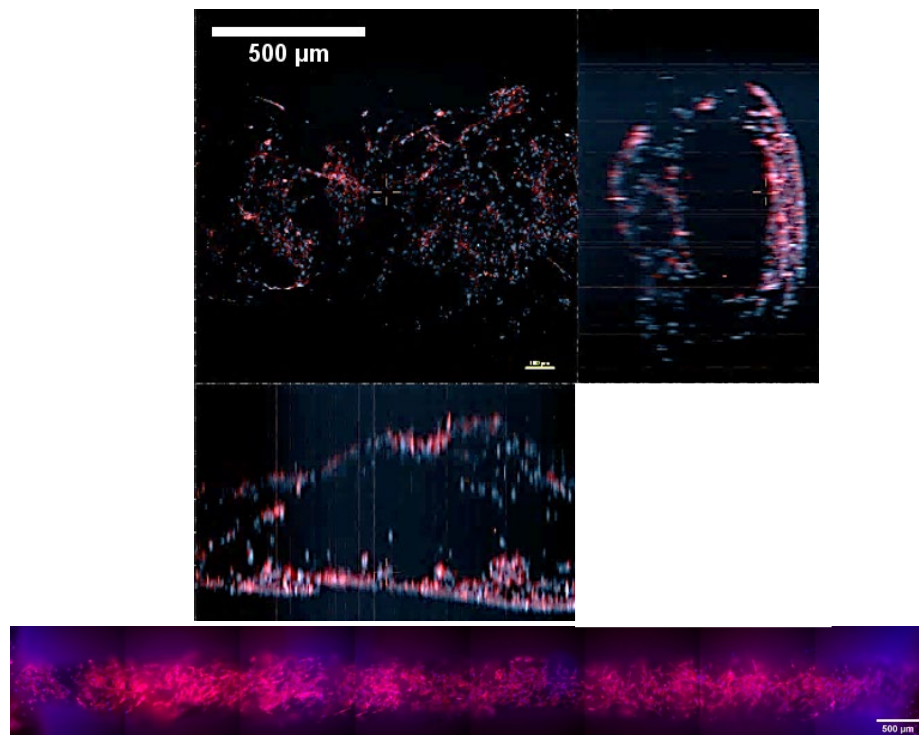*Figure 2.14: HUVECs seeded in GelMa channel adhered throughout the entire channel but jagged edges formed when removing the needle appeared to affect cell adhesion and spreading. Cells were fixed with paraformaldehyde and labeled for nuclei (blue) and actin (red). (Top) Confocal microscopy, 10x magnification, scale bar = 500 μm. (Bottom) Widefield microscopy, 10x magnification, scale bar = 500 μm.*

Figure 2.15: HUVECs seeded in collagen/GelMa channel showed fewer jagged edges as compared to GelMa channels. Cells were fixed with paraformaldehyde and labeled for nuclei (blue) and actin (red). Confocal microscopy, 10x magnification, scale bar = 500 μm.

2.3.5 Subjecting Cells to Flow

Flow experiments were conducted throughout device development, even in cases in which the gels did not seem sufficiently stable to withstand flow. Flow experiments (340 µL/min) using the first collagen device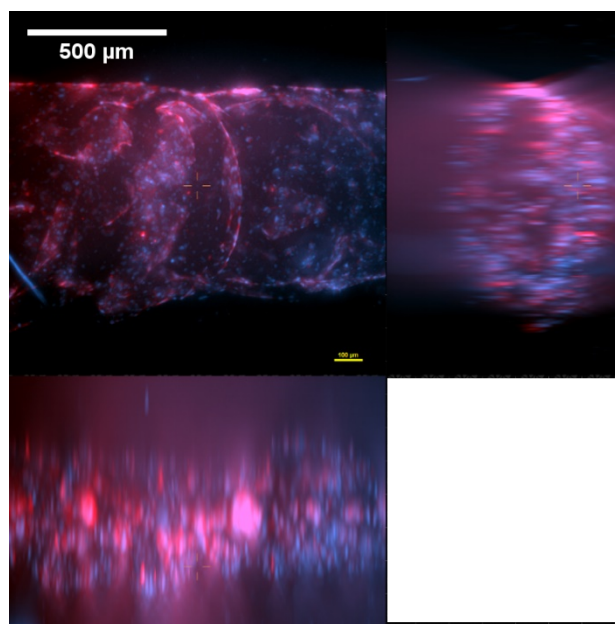 and GFP-mitochondria labeled HUVECs resulted in damage to the collagen gel, often detaching the gel from the PDMS device. However, even in cases where the gel and channel were forced out of their original positions, cell alignment was observed (Figure 2.16).

Later flow experiments using pre-dissolved collagen hydrogels focused on maintaining gel integrity. As such, flow rate was lowered from 340 µL/min as in the previously described experiments to 5 µL/min. Although no alignment was observed, channels could be continuously perfused for up to 48 hours while still maintaining a lumen-like ring structure (Figure 2.17).

The GelMa devices also withstood extended flow durations, so the flowrate was increased to 10 µL/min. Some signs of alignment were observed, but this result was not consistently observed (Figure 2.18). HUVECs were also seeded inside collagen/GelMa channels and subjected to 10 µL/min flow for 48 hours. The cells remained adhered to the channel, and the channel maintained its cylindrical shape. However, no cell alignment was observed in the 1:1 collagen/GelMa blend devices, likely due to the lower flow rate (Figure 2.19). The maximum flowrate achieved while maintaining gel integrity was 20µL/min. This corresponds to a shear stress of 0.03 dyne/cm^2 which is more representative of a pathological shear stresss (~0.01 dyne/cm^2) compared to a physiological shear stress (~12 dyne/cm^2) [73].
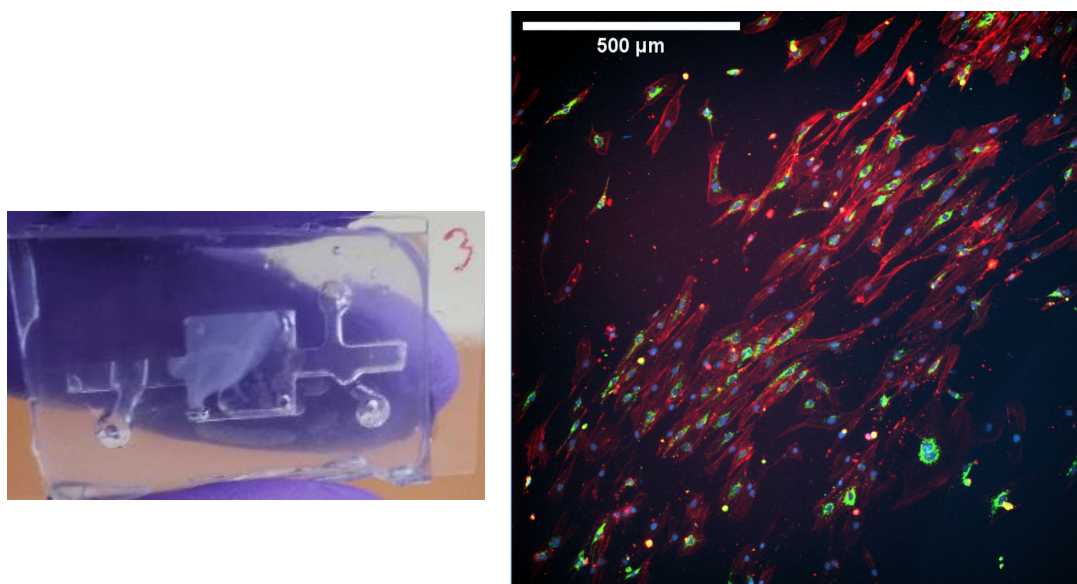
Figure 2.16: GFP-mitochondria labeled HUVECs remained in the collagen channel after being subjected to flow at 340 µL/min for 1 hour. (Left) The high flow rate disrupted the gel, though some parts of the channel could still be imaged. (Right) HUVECs aligned by 1 hour flow. Cells were fixed with paraformaldehyde and labeled for nuclei (blue) and actin (red). Confocal microscopy, 10x magnification, scale bar = 500 µm.
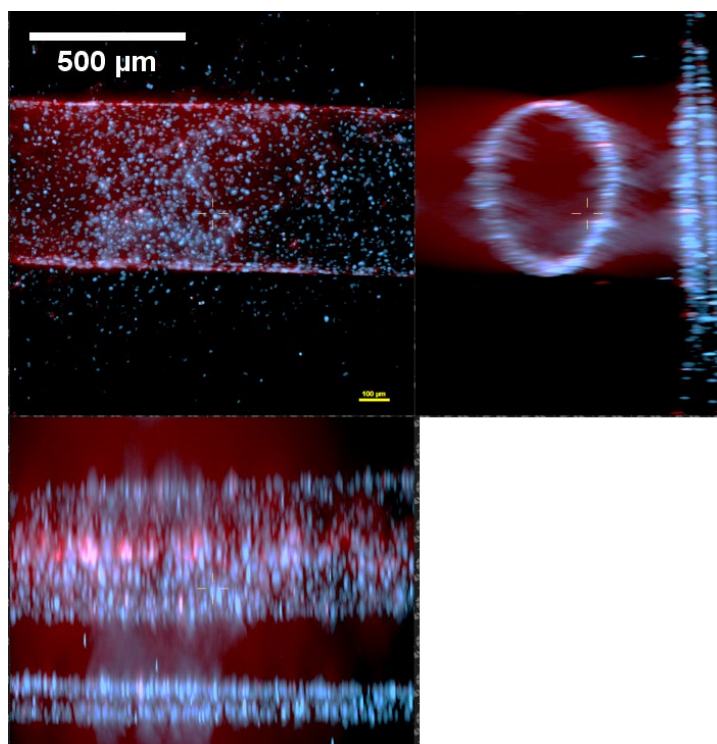
Figure 2.17: HUVECs seeded in collagen channel (pre-dissolved collagen) remained adhered to the intact channel after 5 µL/min flow for 48 hours. Cells were fixed with paraformaldehyde and labeled for nuclei (blue) and actin (red). Confocal microscopy, 10x magnification, scale bar = 500 µm.
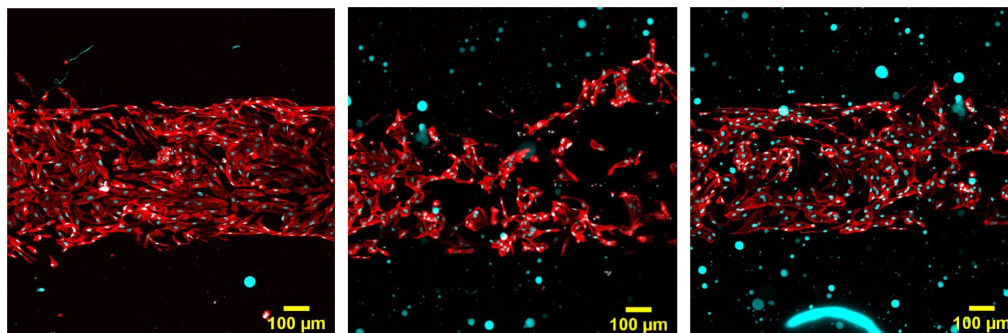
Figure 2.18: HUVECs seeded in three separate GelMa channels remained adhered and showed some sign of cell alignment after 10 µL/min flow for 48 hours. Cells were fixed with paraformaldehyde and labeled for nuclei (blue) and actin (red) Confocal microscopy, 10x magnification, scale bar = 100 µm.

Figure 2.19: HUVECs seeded in three separate collagen/lGelMa channels and subjected to flow at 10 µL/min for 48 hours remained adhered and all channels maintained their form. Cells were fixed with paraformaldehyde and labeled for nuclei (blue) and actin (red). Confocal microscopy, 10x magnification, scale bar = 500 µm.
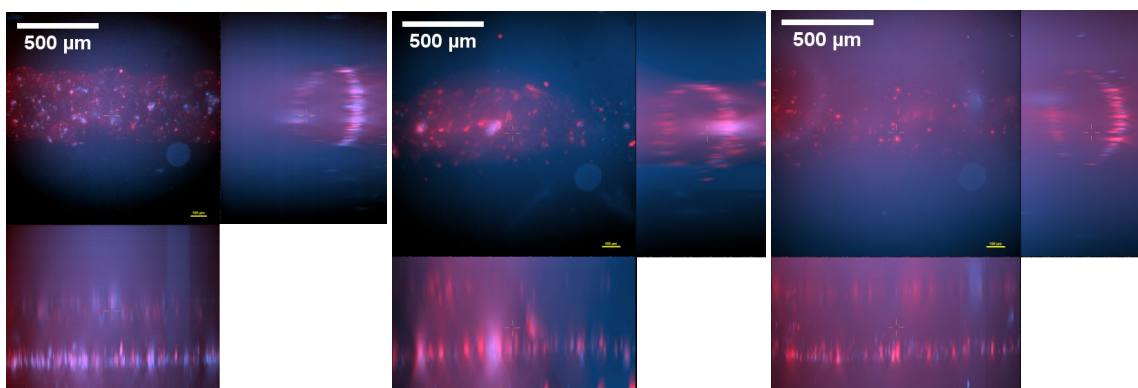
2.4 Discussion

The main challenge addressed in this chapter was establishing a protocol to create a stable, reliable hydrogel that could withstand channel formation and extended flow duration. I first modified the collagen hydrogel gelation protocol to improve the structural integrity of the collagen gels, which were initially fragile and easily destroyed during channel formation and cell seeding. I then explored using a different hydrogel altogether. GelMa hydrogels offered significantly improved gel stability and ease-of-use compared to collagen hydrogels. However, channels formed in GelMa hydrogels had jagged edges along the channel walls. These edges inhibited unidirectional laminar flow through the channel which in turn may have prevented proper cell alignment. It is possible that the rate of gelation contributed to the formation of jagged edges. Compared to the slower gelation of collagen (hours), GelMa hydrogels are crosslinked as quickly as five minutes. This rapid gelation could have increased attachment of the gel to the needle, resulting in jagged edges upon needle removal. In future experiemnts, it may be possible to slow the rate of GelMa crosslinking to reduce the formation of these jagged edges. Finally, collagen and GelMa solutions were mixed to form a hydrogel blend with the gel integrity of GelMa and the smooth-wall channels of collagen.

Other studies have established EC lined hydrogel channels in similar configurations. Chrobak *et al.* developed a collagen channel using a very similar methodology to the artery-on-a-chip device presented here [74]. In their work, they successfully produced a collagen hydrogel channel in a PDMS chip that could be perfused. However, their aim was to form a microvascular tube, and as such their channel diameter was at most 150 μm with a maximum flowrate of 0.4 ml/hr (6.67 μL/min). The larger scale of our artery-on-a-chip

device allows us to study larger vessels and higher flow rates, which are necessary to achieve comparable magnitudes of shear stress, but also requires additional mechanical support, which we have found in collagen/GelMa blend hydrogels.

PDMS is a common feature of many organ-on-a-chip devices. However, in most other devices, more precise and smaller scale fabrication methods are applied, such as soft lithography [75]. In soft lithography, PDMS is cured with a topographical pattern, usually using a silicone master produced with photolithography. Different types of soft lithography will then use this patterned PDMS in different ways. One approach is to bind the patterned PDMS to glass to create microfluidic channels with PDMS walls [76].These types of microfluidic devices offer improved precision and consistency between devices. However, the size scale for this artery-on-a-chip is significantly larger than those types of devices and requires biologically relevant channel walls. While using large molds, as done here, is less precise and consistent between devices compared to soft lithography, it is more sensible for this device as only a PDMS "shell" is required. While other materials or polymers could have fulfilled the same "shell" role as PDMS does in this artery-in-a-chip device, the optical transparency of PDMS is necessary to eventually allow direct visualization of the vessel contraction. It is possible to create PDMS blends with varying mechanical properties. One way to accomplish this would be to vary the ratio of elastomer base and curing agent before PDMS curing. However, even with this tuning, the range of stiffness of PDMS is not compatible with *in vitro* SMC contractility [77].

I now show that collagen/GelMa blends can be used to create stable, smooth-walled hydrogel channels. Collagen/GelMa blend hydrogels have previously been investigated by Stratesteffen *et al.* as a novel 3D printable bioink formulation [78]. Stratesteffen *et al.* used

their collagen/GelMa blends such that individual drops could be crosslinked at a time, which better lends the material to a 3D printing application. Here, an entire hydrogel channel structure was crosslinked and gelled as a single, large construct. An additional benefit of incorporating GelMa into the hydrogel channel is that GelMa is significantly more patternable compared to collagen, and this gel patterning is integral in our approach to aligning muscle cells. GelMa also has natural RGD binding motifs to encourage cell adhesion [79].

These data also show how endothelial cell alignment in the flow direction depends on both the shear stress level and the substrate on which the cells adhere. Specifically, it has been established that laminar flow that induces physiological shear stress on HUVECs aligns them in the flow direction [59]. Flow-based alignment was not observed consistently in the different device iterations for various reasons. For initial collagen devices, the gel stability was not sufficient for extended flow exposure, even at significantly lower than physiological flowrates. GelMa devices suffered from jagged edges that induced disturbed instead of laminar flow. Although it was not observed, collagen/GelMa blend devices were expected to demonstrate cell alignment. The previously mentioned RGD binding motifs present in GelMa provide a clear binding opportunity for $\beta 1$ integrin, which is a sensor of flow direction and essential in EC alignment [80] It is likely that more physiologically relevant flow parameters (increased flow duration and flowrate) are required.

2.5 Conclusion

In this chapter, I present the process of fabricating the hydrogel channel component of the artery-on-a-chip device. Initial devices suffered from a myriad of issues in both the PDMS and collagen hydrogel, but after several iterations and adjustments, I determined a final PDMS device fabrication method and collagen/GelMa blend hydrogel composition that was sufficiently stable to support cell seeding and extended flow exposure. In the next chapter, I describe a novel method for aligning smooth muscle cells inside the channel *in vitro*.

3. Topographical Circumferential Alignment of Vascular Smooth Muscle Cells

3.1 Introduction

In the vascular system, smooth muscle cells (SMCs) are aligned circumferentially about the vessel lumen [81]. This orientation is integral to the function of the muscle cells in constricting and dilating the vessel. Recreating this alignment *in vitro* is therefore a necessity in creating an artery-on-a-chip device that can mimic these vasoconstrictive functions.

Kim *et al.* developed an effective topographical *in vitro* cell alignment platform that serves as a foundation for the work presented here [82]. The platform consists of a flat, nano-patterned surface created using poly(urethane acrylate) molding. This platform is commercially available as patterned culture dishes through Nanosurface Biomedical. However, this nano-patterned surface is only possible in 2D and on rigid substrates.

Methods have been developed for aligning cells, even specifically SMCs, circumferentially about a channel. Choi *et al.* published a method in which microwrinkles were generated along the walls of a PDMS channel, on which SMCs were then seeded [83]. The amplitude and frequency of these microwrinkles could be controlled, with more intense wrinkles aligning SMCs to a greater degree. While this method is arguably simpler and more straightforward than the multi-molding process described in this chapter, PDMS is not a physiologically relevant material. In particular, the stiffness of PDMS would make it impossible to observe *in vitro* contractility.

Since there were no methods to circumferentially pattern SMCs inside a hydrogel channel, I developed a new approach that uses 3D printed molds. These molds are 3D printed using fused deposition modeling as this process inherently creates ridges on the

mold sides that are used as alignment features. I then used this process to pattern flat PDMS and GelMa hydrogels, as well as curved surfaces. Finally, I used a water-dissolvable filament to 3D print sacrificial molds to pattern the inner surface of an entire channel.

3.2 Methods

3.2.1 Smooth Muscle Cell Culture

Human aortic smooth muscle cells (SMCs) were cultured in 100mm culture dishes and maintained with smooth muscle basal media (SmBM, Lonza, CC-3181) supplemented with growth factors (SmGM-2, Lonza, CC-3182). Media was replaced every other day and cells were used between passage 4 and 8. For experiments, cells were detached from the culture dish and counted as described in Chapter 2.

3.2.2 SMC Alignment in 2D with Nano-Patterned Culture Dish

SMCs were seeded into standard 35mm culture dishes (Corning) and commercially available 35mm culture dishes with a nano-patterned culture surface (Nanosurface Biomedical, ANFS-0001-10) specifically designed to align cells in a single direction. This pattern consisted of parallel lines with 800 nm height and 600 nm width. Each line was spaced 800 nm apart. Both types of dishes were coated with rat-tail collagen by preparing a 10 µg/mL solution and covering the bottom of the dishes for at least 30 minutes at 37°C. Cells were seeded at a density of ~90,000 cells/cm^2 and cultured for 24 hours before fixation and imaging.

3.2.3 SMC Alignment on 2D Patterned PDMS

1 cm cubes were 3D printed with 0.15 mm, 0.25 mm, and 0.35 mm layer-thicknesses to act as molds for PDMS patterning. The print parameters were set by the proprietary software of the 3D printer (Afinia, H400). Standard polylactic acid (PLA) filament (Afinia, 25267) was used to print the molds.

A foundational slab of PDMS was first formed in a 100 mm culture dish as described previously. Once fully cured, a wet layer of PDMS was poured onto the slab. The patterning

surfaces of the 3D printed molds were also coated with the wet PDMS. The molds were inverted onto the wet PDMS on the slab, and the entire culture dish was placed in a desiccator to remove air bubbles from the PDMS for 20 to 30 minutes. Any remaining air bubbles were manually removed, and the culture dish was placed an oven set to 80°C for 3 to 24 hours. Once the second layer of PDMS was fully cured, the culture dish was removed from the oven. Using a knife and forceps, the 3D printed molds were separated from the PDMS, leaving PDMS "wells" patterned with the ridge features from the 3D printed molds (Figure 3.1).

Prior to seeding SMCs, the PDMS wells were UV sterilized for 90 minutes, plasma cleaned for 1 minute, and coated with rat-tail collagen (50 µL/mL) for 3 hours at 37°C. 1 × 10^6 SMCs were seeded into each PDMS well. After 24 hours, cells were fixed and labeled as described below.
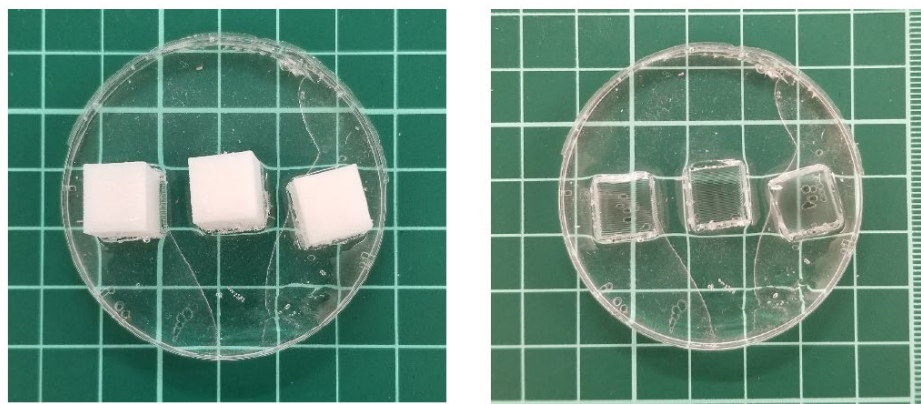
Figure 3.1: Molding process with 3D printed molds. (Left) After PDMS curing, the 3D printed molds were embedded in the PDMS base. (Right) After the 3D printed molds were removed, the PDMS was patterned with alignment ridges. Grid = 10 mm.

3.2.4 SMC Alignment on 2D Patterned GelMa

Patterned PDMS wells were formed as above and left inside the culture dishes. Approximately 1 mL of GelMa solution, prepared with 5% gelatin and 0.3% LAP photoinitiator, was loaded into each well. The culture dish was closed, sealed with parafilm, and UV crosslink for 3 to 5 minutes. Inside a biosafety cabinet, the PDMS was cut and peeled away from the patterned GelMa hydrogel. Each patterned GelMa sample was transferred into a separate well of a 24-well plate. 1×10^6 SMCs were seeded into each well. After 24 hours, cells were fixed and labeled as described below. For imaging, each sample was inverted onto a glass coverslip.

3.2.5 SMC Alignment on Curved Patterned GelMa

Plastic molds were 3D printed in the desired final geometry of the curved patterned GelMa samples. These molds were used to create negative PDMS molds in the same way that 2D patterned PDMS samples were created. The negative PDMS molds were cut into <1 mm squares such that each mold contained three curved half-channel features. Plastic "cages" were printed to keep the GelMa solution in place during crosslinking. A 100 mm culture dish was lined with parafilm to prevent GelMa solution leakage out of the cages. Each cut negative PDMS mold was placed into a cage, with the pattern face up. Approximately 1 mL of GelMa solution with 5% gelatin and 0.3% LAP photoinitiator was loaded into each cage. The solution was crosslinked as described previously. Inside a biosafety cabinet, each cage was inverted such that the flat face of the negative PDMS molds were visible. The negative PDMS molds were carefully peeled away, leaving curved patterned GelMa half-channels samples (Figure 3.2). Each sample was transferred into a separate well of a 24-well plate and seeded with ~5×10^5 cells as described previously.

After 24 hours, cells were fixed and labeled as described below. For imaging, each sample was inverted onto a glass coverslip.

PDMS molding   GelMa crosslinking   Final patterned GelMa
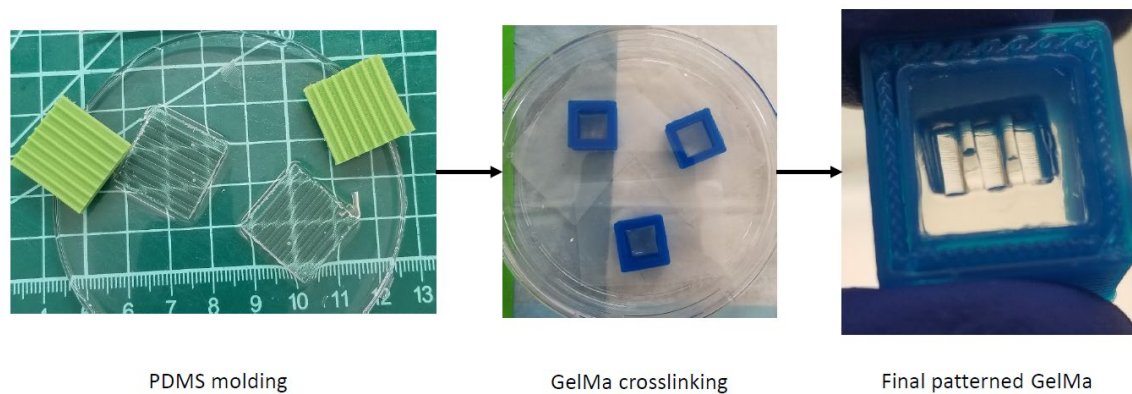
Figure 3.2: Curved GelMa patterning process. (Left) 3D printed molds were used to create PDMS negative molds of the final GelMa hydrogel shape. PDMS was cut to size. (Center) "Cages" were 3D printed to keep GelMa solution in place around PDMS negative molds during crosslinking. (Right) After removal of PDMS negative molds, curved, patterned GelMa hydrogel was revealed.

3.2.6 Channel Patterning with Dissolvable 3D Printed Molds

To pattern the inside of a channel, polyvinyl alcohol (PVA) filament was used to print molds instead of PLA filament. PVA filament is water-soluble and is traditionally used as a support material for 3D printing. 2 mm diameter cylindrical posts were 3D printed at 0.35, 0.25, and 0.15 mm layer thicknesses. The post base allowed the cylinders to stand upright during hydrogel formation. Each post was placed into a well of a 24-well plate and ~1 mL of wet PDMS was added to each well. After incubation at 80°C overnight, water was added to the wells and the well plate was incubated for another overnight period. After the PVA posts fully dissolved, the PDMS channels were cut in half to properly visualize the channel pattern (Figure 3.3). ~5 x 10^5 SMCs were seeded onto the PDMS channel halves.
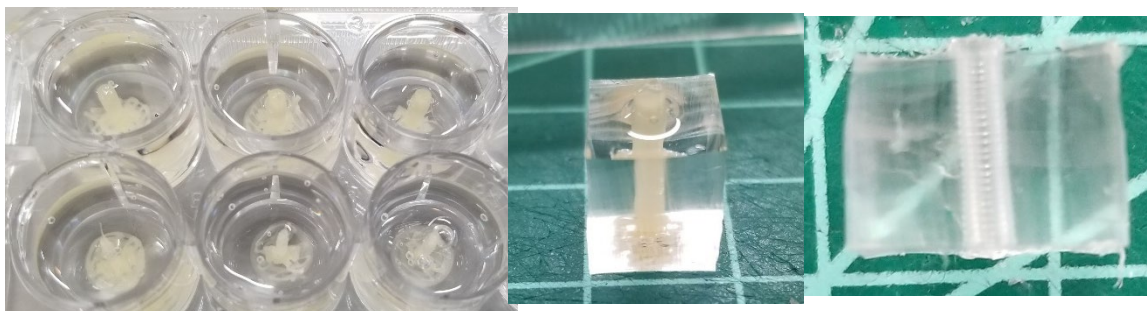
Figure 3.3: Channel patterning process in PDMS. (Left) 3D printed PVA posts were placed in a 24-well plate and surrounded with wet PDMS. (Center) PVA post embedded in cured PDMS. (Right) After dissolving the PVA with water, the PDMS channel retained the 3D printed pattern.

3.2.7 Cell Fixation and Imaging

Cells were washed with cold PBS and fixed with 4% paraformaldehyde (PFA, Invitrogen, FB002) for 15 minutes on ice. The cells were again washed with PBS for 5 minutes. 0.1% Triton X-100 (Alfa Aesar, A16046-AP) was used to permeabilize cells for 5 minutes followed by two additional PBS washes for 5 minutes each. The cells were blocked with 1% bovine serum albumin (BSA, Sigma Aldrich, A9418) for 30 minutes and then stained with 0.05% Hoechst (Invitrogen, H3570) and 1.25% rhodamine phalloidin (Biotium, 00027) to label nuclei and actin, respectively. A confocal laser scanning microscope (Nikon, Eclipse Ti2-E) was used to image the cells. Images were obtained at 10x and 20x magnification over a range of 300-1000 μm in depth. 100 z-stacks were acquired to visualize cell alignment along the various patterns and ridge features.

3.2.8 Alignment Quantification

Cell alignment was quantified using MatFiber for actin. MatFiber is software developed in MATLAB and originally used to quantify collagen fiber orientation in myocardial scar tissue in rats after myocardial infarction [84]. Briefly, the software divides an input image into square subregions. Each subregion is assigned a vector based on an intensity gradient detection algorithm [85]. The vector angles are calculated to quantify the overall orientation of the image. Images are transformed such that expected alignment (direction of alignment features) is 0°.

3.3 Results

3.3.1 SMC Alignment in 2D with Nano-Patterned Culture Dish

To demonstrate the feasibility of aligning SMCs in 2D, cells were seeded in commercially available culture dishes with a nano-patterned culture surface. Cells were also seeded in standard, un-patterned culture dishes as a negative control. As expected, when seeded on the un-patterned culture dish, no alignment was observed. In contrast, cells seeded on the nano-patterned culture dished showed significant alignment in the direction of the patterned lines (Figure 3.4) .
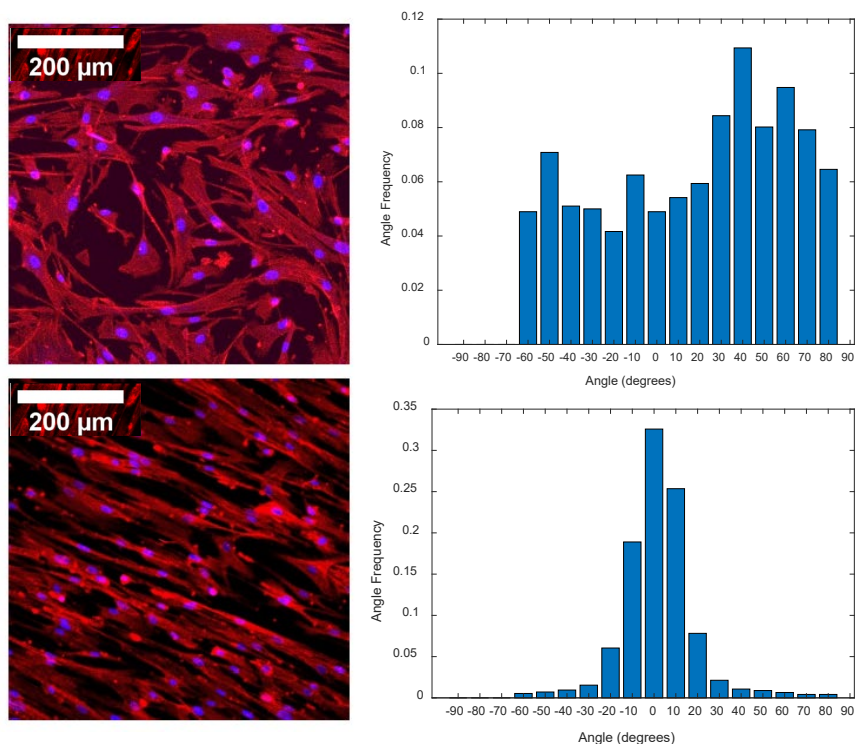

Figure 3.4: SMCs seeded onto nano-patterned culture surfaces aligned in the pattern direction. (Left) Confocal microscopy images of SMCs labeled for nuclei (blue) and actin (red). (Right) Alignment quantification of SMCs seeded in an unpatterned culture dish (top) and a nano-patterned culture dish (bottom). Scale bar = 200μm

3.3.2 SMC Alignment on 2D Patterned PDMS

Although SMCs clearly demonstrated alignment due to the topographic cues of the nano-patterned culture surface, this rigid 2D surface is far from the final desired artery-on-a-chip device. To begin working towards the desired circumferential alignment, topographical patterned PDMS was explored because of the ability to mold PDMS into customizable forms.

First, 2D topographical patterning of PDMS was accomplished by using 3D printed molds in which the ridge dimensions were controlled by adjusting the layer-thickness of the 3D printer, which in turn controlled the pattern imparted onto the PDMS surface (Figure 3.5). Three molds were printed with different layer-thicknesses to determine the effect on cell alignment.

SMCs aligned to a high degree on the patterned PDMS (Figure 3.6), considering that the ridge size and spacing was much larger compared to the nano-patterned culture dishes. The layer-thickness of each sample did not significantly change the degree of alignment (Figure 3.7). These experiments demonstrated that PDMS could be patterned using 3D printed molds and that this pattern could effectively align SMCs.

0.35mm   0.25mm   0.15mm
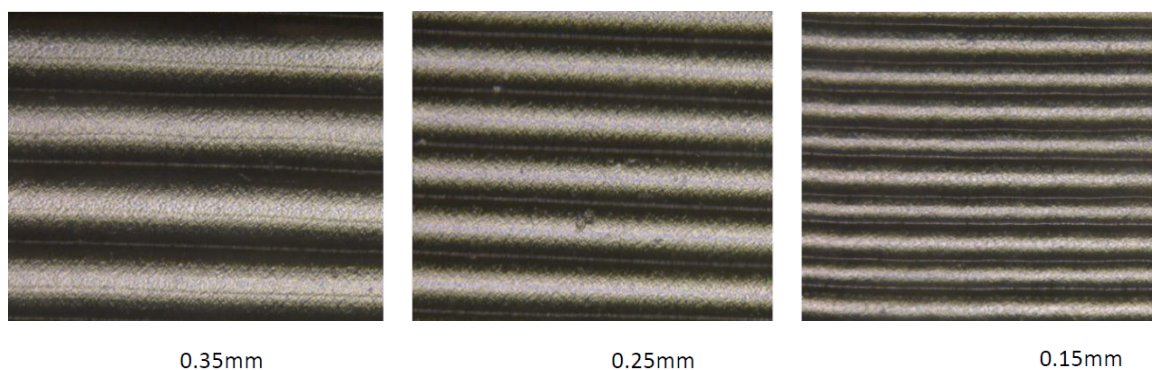
Figure 3.5: Phase contrast images of alignment features in patterned PDMS formed using 3D printed PLA molds. Phase contrast microscopy, 5x magnification.
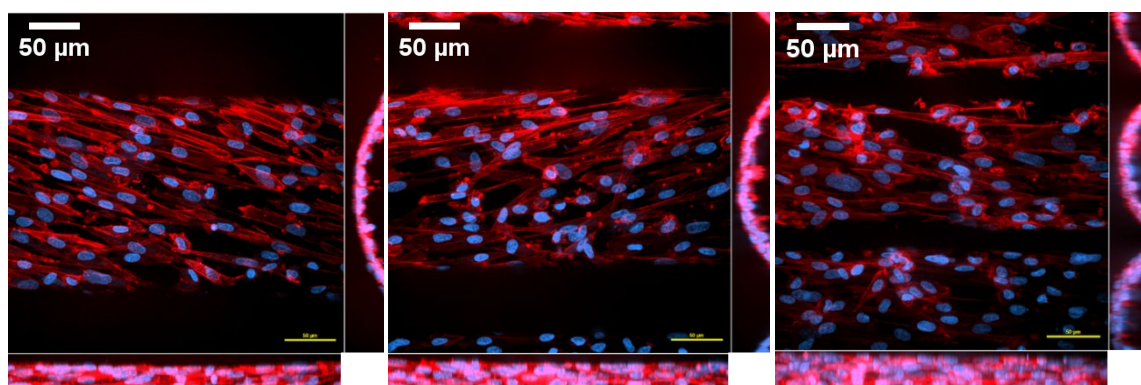

Figure 3.6: SMCs aligned with the ridges on patterned PDMS. Cells were fixed with paraformaldehyde and labeled for nuclei (blue) and actin (red). Confocal microscopy, 60x magnification, scale bar = 50 μm.
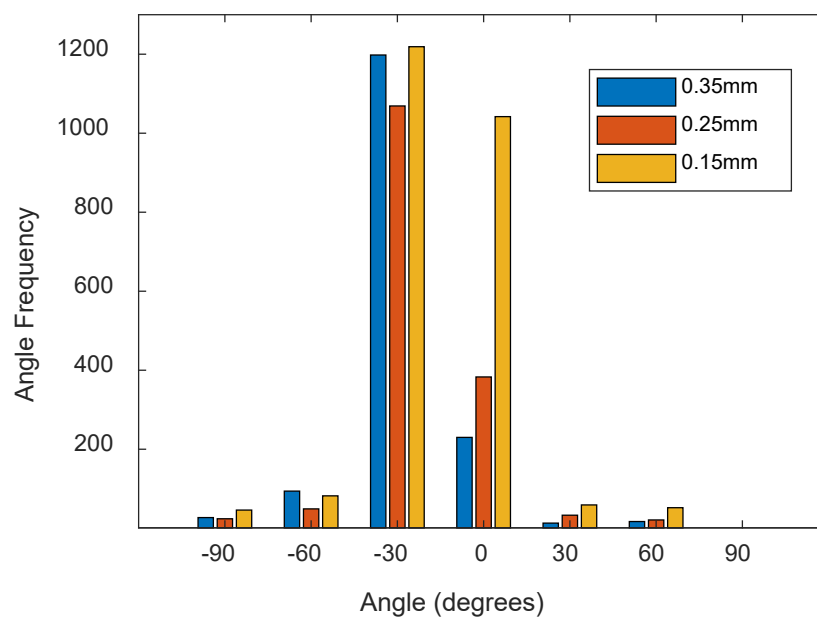

Figure 3.7: SMC aligned to a similar degree on patterned PDMS of different ridge size.

3.3.3 SMC Alignment on 2D Patterned GelMa

Although the PDMS curing process lends itself to more easily forming 3D structures, its mechanical and biological properties do not make it an ideal substrate on which to culture SMCs with the intent to induce and observe contractility. GelMa presented an appealing combination of 3D structure formation and physiological relevance, both biologically and mechanically. The following experiments were designed to determine the feasibility of patterning GelMa hydrogels and if possible, if patterned GelMa surfaces could align SMCs as in previous experiments.

Initial attempts at patterning GelMa were carried out nearly identically to the process developed to pattern PDMS using 3D printed molds. However, removing the rigid plastic molds from the soft GelMa hydrogels was not possible without significantly disrupting the hydrogel, damaging any pattern that may have formed. To address this issue, an intermediate PDMS molding step was added. The 3D printed molds were used to pattern PDMS as before, but these patterned PDMS samples were then used to ultimately pattern the GelMa hydrogels. The pliable nature of PDMS allowed the PDMS molds to be cut and peeled away from the GelMa hydrogels with minimal damage to the pattern (Figure 3.8).

When seeding SMCs onto these 2D patterned GelMa samples, less alignment was observed compared to SMCs seeded on patterned PDMS samples (Figure 3.9). However, alignment was still observed, primarily in the 0.15 mm layer-thickness samples. These experiments established that GelMa could feasibly be patterned using 3D printed molds and PDMS intermediate molds.

Figure 3.8: GelMa hydrogel sample patterned using 0.35mm layer-thickness 3D printed mold. GelMa solution was loaded onto patterned PDMS samples and crosslinked in place. Peeling away the PDMS revealed the patterned GelMa sample.
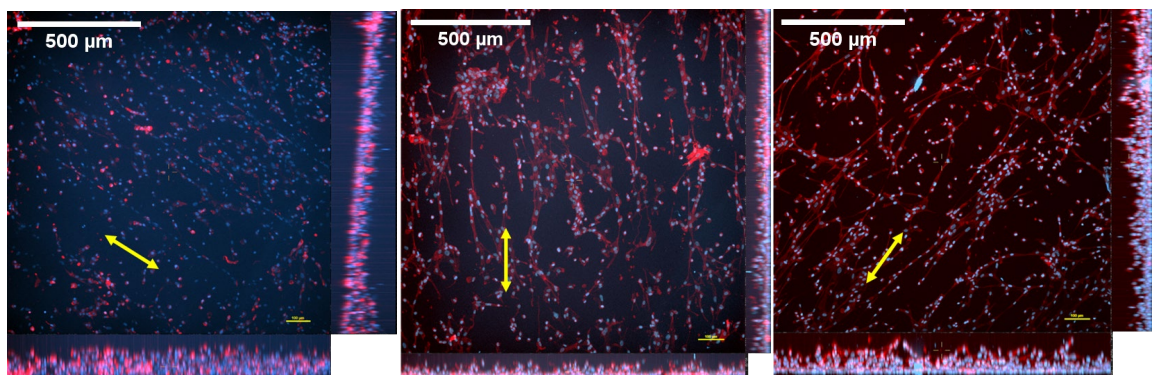
Figure 3.9: SMCs seeded on patterned GelMa samples showed less alignment than cells seeded onto PDMS. Cells were fixed with paraformaldehyde and labeled for nuclei (blue) and actin (red). Yellow arrows indicate direction of alignment features. Confocal microscopy, 10x magnification, scale bar = 500 μm.
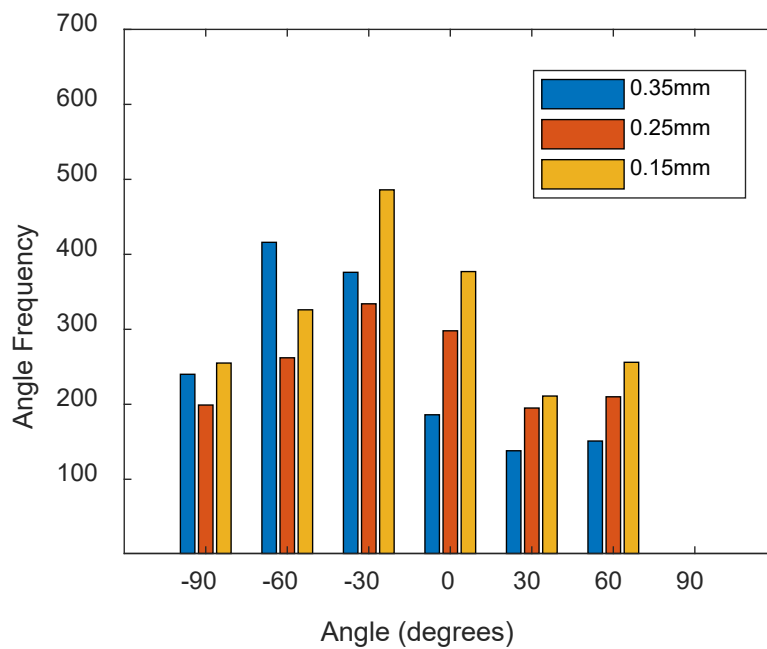
Figure 3.10 SMC showed less overall alignment on GelMa, though the trend of increased alignment with decreasing layer thickness remained.

3.3.4 SMC Alignment on Curved Patterned GelMa

The final desired SMC orientation in the artery-on-a-chip device is circumferential alignment inside the channel. The next step towards accomplishing this was to adapt the GelMa patterning process to create curved patterned surfaces. In these experiments, a half channel structure was attempted to determine if curvature would affect the patterning process.

SMCs seeded onto these curved patterned GelMa surfaces again demonstrated some alignment (Figure 3.11). Compared to the 2D patterned GelMa samples, the SMC alignment on curved patterned GelMa samples was again diminished in alignment and consistency as more or less alignment was observed in different areas of the same sample (Figure 3.12).

0.35mm   0.25mm   0.15mm
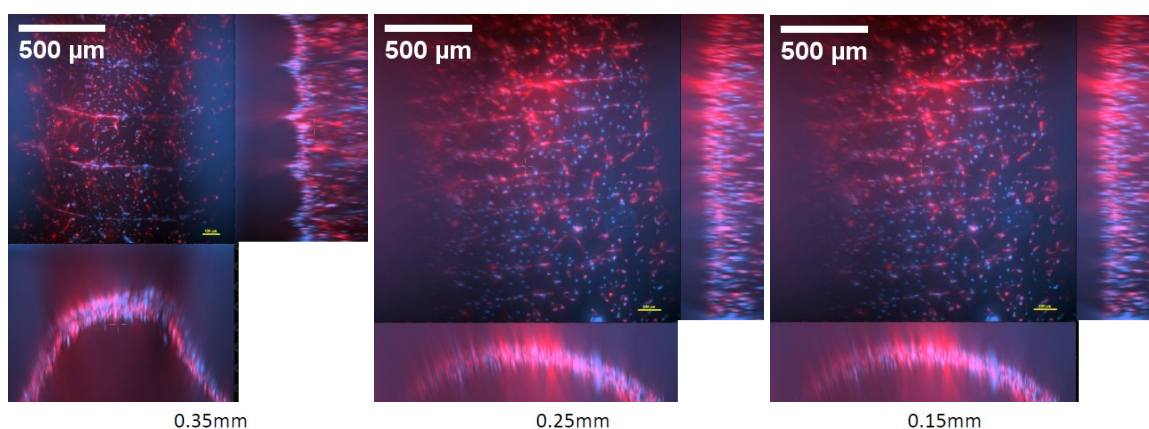
Figure 3.11: SMCs seeded on curved patterned GelMa samples showed some circumferential alignment. Curved surfaces were fabricated using a PDMS negative mold. The alignment features were inherent to the PDMS mold. SMC were fixed with paraformaldehyde and labeled for nuclei (blue) and actin (red). Confocal microscopy, 10x magnification, scale bar = 500 μm.

58
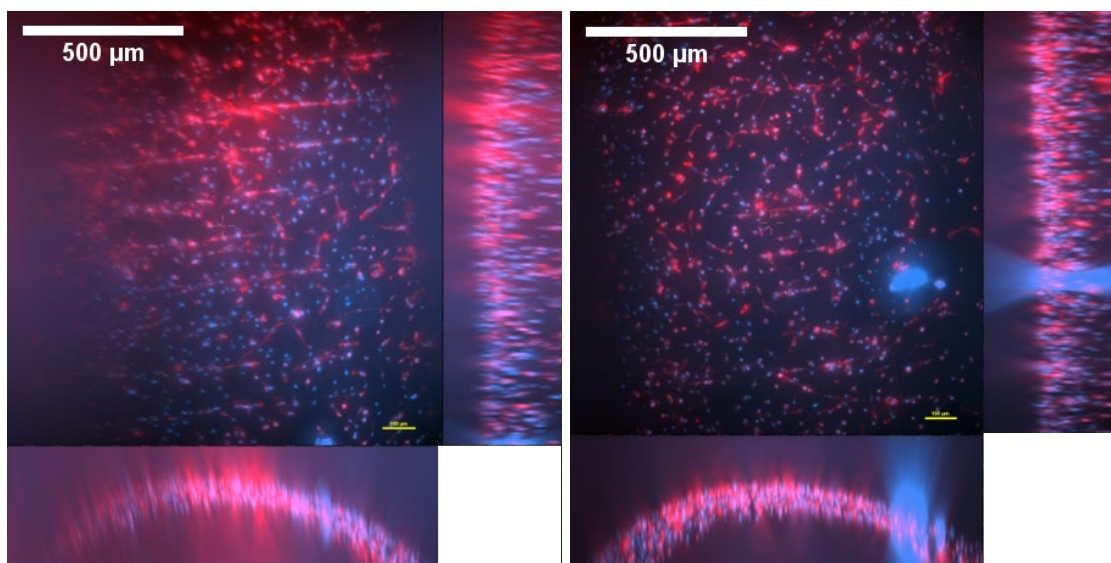
Figure 3.12: SMCs seeded on curved patterned GelMa samples patterned with 0.15 mm layer-thickness showed some areas with circumferential alignment but also areas without alignment. Curved surfaces were fabricated using a PDMS negative mold. The alignment features were inherent to the PDMS mold. SMC were fixed with paraformaldehyde and labeled for nuclei (blue) and actin (red). Confocal microscopy, 10x magnification, scale bar = 500 µm.
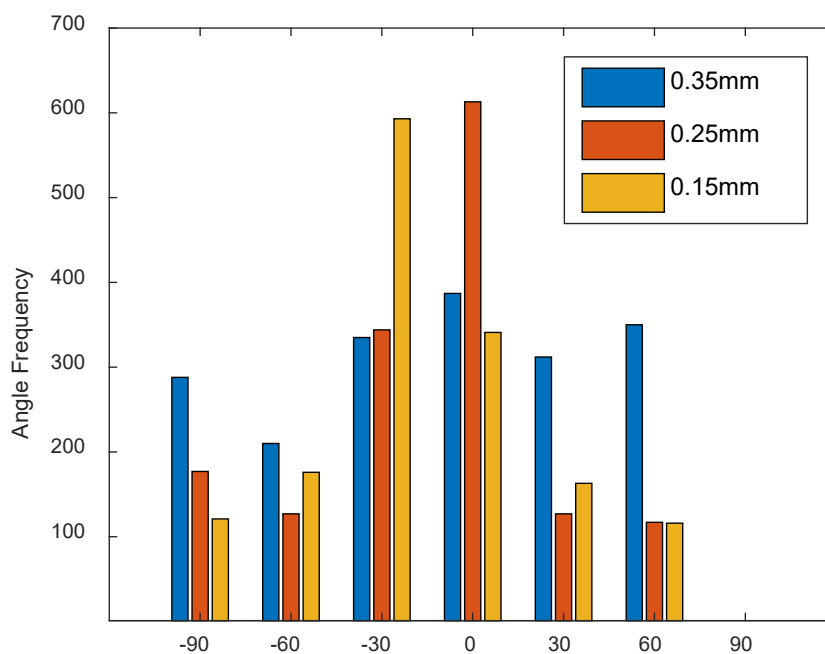
Figure 3.13: SMC aligned to on curved GelMa surfaces at 0.25mm and 0.15mm layer thicknesses, but not at 0.35mm.

3.3.5 Channel Patterning with Dissolvable 3D Printed Molds

After dissolving the PVA molds, the PDMS channels were clearly patterned by the sacrificial molds. However, due to the print quality of the molds, the patterns were not as robust as previous samples (Figure 3.14).

| 0.35mm | 0.25mm | 0.15mm |
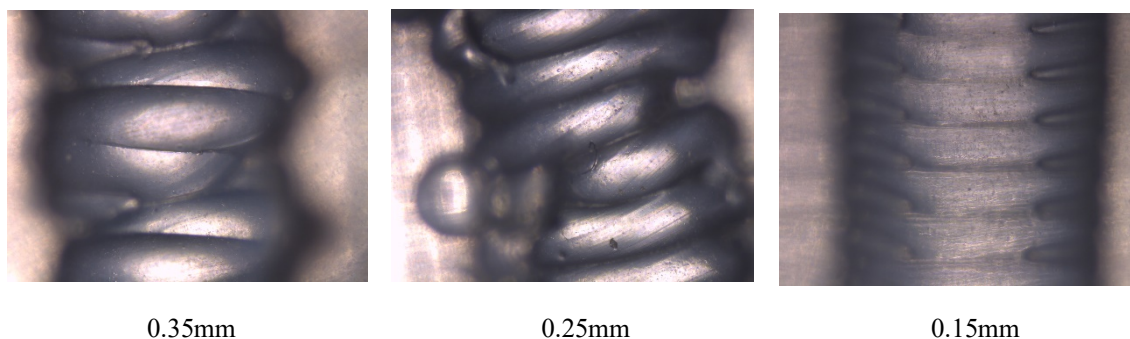
Figure 3.14: PDMS channels patterned with dissolvable PVA mold. 0.35 mm and 0.25 mm layer-thickness molds printed in non-uniform layers. Phase contrast microscopy, 5x magnification.

3.4 Discussion

With these experiments, I confirmed that SMCs can be aligned with a simple process using 3D printed molds. Of the topographical patterns tested in this chapter, Nanosurface Biomedical's nano-patterned cultured surfaces had the finest alignment features, with the smallest feature size being 600 nm. The fine feature size resulted in the clearest cell alignment. PDMS offered a more customizable and facile patterning method using 3D printed molds. With this 3D printed molding process, I created alignment features in both flat and curved PDMS samples. I then established that these patterns were sufficient to align SMCs. Although the degree of alignment of cells on PDMS samples was lower than that of cells on the nano-patterned culture dish, appreciably alignment was still observed. However, PDMS is not a suitable material for the artery-on-a-chip device as it is too stiff to allow visible SMC contraction. Therefore, patterning GelMa hydrogels was attempted. With a few additional steps to the 3D printed molding process, I created similar alignment features on flat and curved GelMa surfaces. Again, the cells alignment on these samples decreased compared to cells on PDMS samples, but the GelMa hydrogel composition could be further tuned to improve pattern transfer. Finally, I began adapting this 3D printed molding process towards the ultimate goal of aligning SMCs circumferentially inside a channel. Using 3D printed PVA molds, I was able to pattern a PDMS channel with similar alignment features to that of the flat and curved samples. The alignment features were not as robust as previous experiments, but this could be remedied with higher quality 3D printing.

To apply this method to the artery-on-a-chip device would first require establishing the channel formation process in GelMa. Based on the success of patterning the PDMS channel

and of patterning the flat and curved GelMa samples, it appears likely that channel patterning in GelMa is possible with this method. Some additional considerations would have to be made regarding certain parameters of the 3D printed molding process. The print resolution and mold diameter are closely related. Smaller diameter molds require a more precise 3D printer for consistency among prints, especially at different layer-thicknesses. Although layer-thicknesses did not appear to affect cell alignment, conditions in the artery-on-a-chip device may cause certain ridge sizes to be more or less effective at aligning cells. For instance, the combined effects of layer-thickness and flow would have to be investigated. Similarly, the gel composition could affect ridge formation. While GelMa could be patterned and demonstrated cell alignment, Chapter 2 experiments indicated that GelMa alone was not compatible with the channel formation process. A collagen/GelMa blend could be equally patternable, as long as its stiffness is similar to GelMA alone.

This 3D printed molding process is substantially more cost effective compared to techniques that achieve similar results. For example, the nano-patterned culture surfaces manufactured by Nanosurface Biomedical cost $160.00 per 24-well plate. 3D printed molding does require an initial startup cost to acquire a 3D printer ($500 and up); alternatively, most universities have core facilities for 3D printing. In addition, 3D printed molds can also be used several times and can be customized to the application. Non-topographical alignment methods, such as electrical and mechanical stimulation, require more complex equipment, limit the conditions in which cells can be cultured, and may affect cell physiology in undesired ways that could affect cell function. This simple and cost-effective patterning method could make the artery-on-a-chip accessible to many laboratories so that these devices can be readily, and consistently, reproduced.

3.5 Conclusion

In this chapter, I present a novel process of aligning SMCs circumferentially inside a channel as they would ultimately be required in the artery-in-a-chip device. Cells were first aligned topographically with commercially available rigid pre-patterned surfaces to establish a baseline cell alignment. Then, 3D printed molds were used in conjunction with PDMS to develop a simple and cost effect method of topographically aligning cells. I demonstrated that this method could not only be used to align SMCs in 2D, but also on curved surfaces. Although the effectiveness of cell alignment decreased on softer hydrogels, alignment was still observed and the patterning process can be tuned as necessary for future experiments.

4. Conclusions and Future Work

4.1 Conclusions

In this thesis, several important steps were taken towards creating a contractile artery-on-a-chip using human ECs and SMCs. In Aim 1, an optically transparent PDMS-based device was used as the artery-on-a-chip foundation. Cells were seeded in a soft hydrogel channel that would allow SMC contraction to produce visible changes in diameter, a requirement of pressure myography. The hydrogel composition was changed, as early compositions were not sufficiently stable to withstand channel formation and extended flow. A blend of collagen and GelMa was chosen as the final hydrogel composition. GelMa offers a facile crosslinking method, high stability, and strong attachment to the PDMS device, in addition to physiologically relevant binding motifs. Using GelMa alone, however, resulted in hydrogel channels with jagged edges that hindered cell adherence and alignment. Blending GelMa together with collagen lessened the intensity of these jagged edges, while still having the benefits of GelMa.

Another important step towards achieving the contractile artery-on-a-chip was the development of a novel method to topographically align SMCs circumferentially. 3D printing is a growing technology and, while not as precise, is much more accessible than microfabrication methods. 3D printed molds were successfully used to pattern PDMS substrates, and SMCs seeded on these substrates aligned with the topographical patterns. By simply changing the shape of the 3D printed mold, even curved surfaces were fabricated that supported cell alignment features. This was established in both PDMS and GelMa hydrogel samples, further speaking to the versatility of this method. Even further still, sacrificial molds 3D printed using PVA filament. This water-soluble filament does not

significantly complicate or increase the expense of this method, but greatly widens its possible uses. In this case, a 3D printed cylindrical sacrificial mold was used to pattern the inner walls of a channel with alignment features.

4.2 Future Work

The natural progression of the two aims detailed here is to co-culture ECs and SMCs within the hydrogel channel. This would begin with first incorporating the hydrogel patterning method developed in Aim 2 into the PDMS device. This could be done with minor changes to the hydrogel formation process. When SMCs are circumferentially aligned inside the channel, the ECs would be seeded in a monolayer on top of the SMCs and aligned axially using fluid flow. The next major step would be to validate artery-on-a-chip vasodilation and vasoconstriction with pressure myography of harvested tissue samples. While the artery-on-a-chip device is not expected to respond with the same magnitude as a harvested tissue sample, it should at least follow the same type of response as a native artery.

With a validated, contractile artery-on-a-chip device, more comprehensive topics could be investigated. Related to atherosclerosis, the device could be modified to create branched vessels to observe differences between unidirectional and non-unidirectional flow. The time scale for the current device is limited to 48 hours which is signifncantly shorter than the time required for atherosclerosis to develop naturally (decades). However, disease conditions could be accelerated through the use of NO scavengers to reduce NO bioavailability. Additionally, the role of vascular-adjacent tissues could be better studied by introducing these cells or tissues to the hydrogel. The effects of perivascular adipose

tissue inflammation on vasoconstriction and vasodilation, for example, could be studied in a much more controlled environment with this device.

References

[1] L. J. Laslett *et al.*, "The worldwide environment of cardiovascular disease: Prevalence, diagnosis, therapy, and policy issues: A report from the american college of cardiology," *J. Am. Coll. Cardiol.*, vol. 60, no. 25 SUPPL., 2012, doi: 10.1016/j.jacc.2012.11.002.

[2] World Health Organization, "Global Atlas on Cardiovascular Disease Prevention And Control. Policies, Strategies and Interventions," *Iraq*, p. 164, 2011.

[3] F. Schaftenaar, V. Frodermann, J. Kuiper, and E. Lutgens, "Atherosclerosis: The interplay between lipids and immune cells," *Curr. Opin. Lipidol.*, vol. 27, no. 3, pp. 209–215, 2016, doi: 10.1097/MOL.0000000000000302.

[4] B. Emini Veseli *et al.*, "Animal models of atherosclerosis," *Eur. J. Pharmacol.*, vol. 816, pp. 3–13, 2017, doi: 10.1016/j.ejphar.2017.05.010.

[5] K. J. Moore, F. J. Sheedy, and E. A. Fisher, "Macrophages in atherosclerosis: A dynamic balance," *Nat. Rev. Immunol.*, vol. 13, no. 10, pp. 709–721, 2013, doi: 10.1038/nri3520.

[6] Y. Wang *et al.*, "Smooth Muscle Cells Contribute the Majority of Foam Cells in ApoE (Apolipoprotein E)-Deficient Mouse Atherosclerosis," *Arterioscler. Thromb. Vasc. Biol.*, vol. 39, no. 5, pp. 876–887, 2019, doi: 10.1161/ATVBAHA.119.312434.

[7] M. K. Pugsley and R. Tabrizchi, "The vascular system: An overview of structure and function," *J. Pharmacol. Toxicol. Methods*, 2000, doi: 10.1016/S1056-8719(00)00125-8.

[8] W. D. Tucker and K. Mahajan, *Anatomy, Blood Vessels*. 2018.

[9]   E. J. Gussenhoven *et al.*, "Arterial wall characteristics determined by intravascular ultrasound imaging: An in vitro study," *J. Am. Coll. Cardiol.*, vol. 14, no. 4, pp. 947–952, 1989, doi: 10.1016/0735-1097(89)90471-3.

[10]   H. Watanabe, "Endothelial dysfunction and cardiovascular diseases," *Japanese Pharmacol. Ther.*, vol. 28, no. 6, pp. 441–443, 2000, doi: 10.5339/gcsp.2014.43.

[11]   P. M. Vanhoutte, H. Shimokawa, M. Feletou, and E. H. C. Tang, "Endothelial dysfunction and vascular disease – a 30th anniversary update," *Acta Physiologica*. 2017, doi: 10.1111/apha.12646.

[12]   Y. Zhao, P. M. Vanhoutte, and S. W. S. Leung, "Vascular nitric oxide: Beyond eNOS," *Journal of Pharmacological Sciences*, vol. 129, no. 2. pp. 83–94, 2015, doi: 10.1016/j.jphs.2015.09.002.

[13]   A. Krüger-Genge, A. Blocki, R. P. Franke, and F. Jung, "Vascular endothelial cell biology: An update," *International Journal of Molecular Sciences*, vol. 20, no. 18. 2019, doi: 10.3390/ijms20184411.

[14]   J. G. McCarron, M. D. Lee, and C. Wilson, "The Endothelium Solves Problems That Endothelial Cells Do Not Know Exist," *Trends in Pharmacological Sciences*, vol. 38, no. 4. pp. 322–338, 2017, doi: 10.1016/j.tips.2017.01.008.

[15]   F. E. Curry and R. H. Adamson, "Endothelial glycocalyx: Permeability barrier and mechanosensor," *Ann. Biomed. Eng.*, vol. 40, no. 4, pp. 828–839, Apr. 2012, doi: 10.1007/s10439-011-0429-8.

[16]   A. I. Barakat, "Responsiveness of vascular endothelium to shear stress: Potential role of ion channels and cellular cytoskeleton (Review)," *Int. J. Mol. Med.*, vol. 4, no. 4, pp. 323–332, 1999, doi: 10.3892/ijmm.4.4.323.

[17] Y. J. Chiu, K. I. Kusano, T. N. Thomas, and K. Fujiwara, "Endothelial cell-cell adhesion and mechanosignal transduction," *Endothel. J. Endothel. Cell Res.*, vol. 11, no. 1, pp. 59–73, 2004, doi: 10.1080/10623320490432489.

[18] E. A. Osborn, A. Rabodzey, C. F. Dewey, and J. H. Hartwig, "Endothelial actin cytoskeleton remodeling during mechanostimulation with fluid shear stress," *Am. J. Physiol. - Cell Physiol.*, vol. 290, no. 2, pp. 444–452, 2006, doi: 10.1152/ajpcell.00218.2005.

[19] U. Förstermann and T. Münzel, "Endothelial nitric oxide synthase in vascular disease: From marvel to menace," *Circulation*, vol. 113, no. 13, pp. 1708–1714, 2006, doi: 10.1161/CIRCULATIONAHA.105.602532.

[20] D. Tousoulis, A.-M. Kampoli, C. Tentolouris Nikolaos Papageorgiou, and C. Stefanadis, "The Role of Nitric Oxide on Endothelial Function," *Curr. Vasc. Pharmacol.*, vol. 10, no. 1, pp. 4–18, 2011, doi: 10.2174/157016112798829760.

[21] M. C. Verhaar, P. E. Westerweel, A. J. Van Zonneveld, and T. J. Rabelink, "Free radical production by dysfunctional eNOS," *Heart*, vol. 90, no. 5, pp. 494–495, 2004, doi: 10.1136/hrt.2003.029405.

[22] I. Fleming and R. Busse, "Signal transduction of eNOS activation," *Cardiovasc. Res.*, vol. 43, no. 3, pp. 532–541, 1999, doi: 10.1016/S0008-6363(99)00094-2.

[23] J. N. Wilcox *et al.*, "Expression of multiple isoforms of nitric oxide synthase in normal and atherosclerotic vessels," *Arterioscler. Thromb. Vasc. Biol.*, vol. 17, no. 11, pp. 2479–2488, 1997, doi: 10.1161/01.ATV.17.11.2479.

[24] P. Marchio, S. Guerra-Ojeda, J. M. Vila, M. Aldasoro, V. M. Victor, and M. D. Mauricio, "Targeting early atherosclerosis: A focus on oxidative stress and

inflammation," *Oxid. Med. Cell. Longev.*, vol. 2019, no. Ldl, 2019, doi: 10.1155/2019/8563845.

[25] S. Čejková, I. Králová-Lesná, and R. Poledne, "Monocyte adhesion to the endothelium is an initial stage of atherosclerosis development," *Cor Vasa*, vol. 58, no. 4, pp. e419–e425, 2016, doi: 10.1016/j.crvasa.2015.08.002.

[26] J. J. Chiu, S. Usami, and S. Chien, "Vascular endothelial responses to altered shear stress: Pathologic implications for atherosclerosis," *Ann. Med.*, vol. 41, no. 1, pp. 19–28, 2009, doi: 10.1080/07853890802186921.

[27] M. W. Peters, P. B. Canham, and H. M. Finlay, "Circumferential alignment of muscle cells in the tunica media of the human brain artery," *J. Vasc. Res.*, vol. 20, no. 5, pp. 221–233, 1983, doi: 10.1159/000158475.

[28] R. M. Touyz *et al.*, "Vascular smooth muscle contraction in hypertension," *Cardiovasc. Res.*, vol. 114, no. 4, pp. 529–539, 2018, doi: 10.1093/cvr/cvy023.

[29] B. G. Allen and M. P. Walsh, "The biochemical basis of the regulation of smooth-muscle contraction," *Trends Biochem. Sci.*, vol. 19, no. 9, pp. 362–368, 1994, doi: 10.1016/0968-0004(94)90112-0.

[30] R. C. Webb, "Smooth muscle contraction and relaxation," *Am. J. Physiol. - Adv. Physiol. Educ.*, vol. 27, no. 1–4, pp. 201–206, 2003, doi: 10.1152/advan.00025.2003.

[31] S. M. Yuan, "α-Smooth muscle actin and ACTA2 gene expressions in vasculopathies," *Brazilian J. Cardiovasc. Surg.*, vol. 30, no. 6, pp. 644–649, 2015, doi: 10.5935/1678-9741.20150081.

[32] M. M. Kockx, G. R. Y. De Meyer, J. Muhring, W. Jacob, H. Bult, and A. G. Herman,

"Apoptosis and related proteins in different stages of human atherosclerotic plaques," *Circulation*, 1998, doi: 10.1161/01.CIR.97.23.2307.

[33] S. D. Cushing *et al.*, "Minimally modified low density lipoprotein induces monocyte chemotactic protein 1 in human endothelial cells and smooth muscle cells," *Proc. Natl. Acad. Sci. U. S. A.*, vol. 87, no. 13, pp. 5134–5138, 1990, doi: 10.1073/pnas.87.13.5134.

[34] G. L. Basatemur, H. F. Jørgensen, M. C. H. Clarke, M. R. Bennett, and Z. Mallat, "Vascular smooth muscle cells in atherosclerosis," *Nat. Rev. Cardiol.*, vol. 16, no. 12, pp. 727–744, 2019, doi: 10.1038/s41569-019-0227-9.

[35] Y. Vengrenyuk *et al.*, "Cholesterol loading reprograms the microRNA-143/145-Myocardin axis to convert aortic smooth muscle cells to a dysfunctional macrophage-like phenotype," *Arterioscler. Thromb. Vasc. Biol.*, 2015, doi: 10.1161/ATVBAHA.114.304029.

[36] S. S. M. Rensen, P. A. F. M. Doevendans, and G. J. J. M. Van Eys, "Regulation and characteristics of vascular smooth muscle cell phenotypic diversity," *Netherlands Hear. J.*, vol. 15, no. 3, pp. 100–108, 2007, doi: 10.1007/BF03085963.

[37] M. Kelm, "Nitric oxide metabolism and breakdown," *Biochimica et Biophysica Acta - Bioenergetics*, vol. 1411, no. 2–3. pp. 273–289, 1999, doi: 10.1016/S0005-2728(99)00020-1.

[38] P. Vallance *et al.*, "Direct measurement of nitric oxide in human beings," *Lancet*, vol. 346, no. 8968, pp. 153–154, 1995, doi: 10.1016/S0140-6736(95)91211-8.

[39] M. J. Serpe and X. Zhang, "and Application of Determination of Nitric Oxide," *Nitric Oxide*, pp. 465–488, 2006.

[40] C.-Z. Li, S. Alwarappan, W. Zhang, N. Scafa, and X. Zhang, "Metallo Protoporphyrin Functionalized Microelectrodes for Electrocatalytic Sensing of Nitric Oxide," *Am. J. Biomed. Sci.*, pp. 274–282, 2009, doi: 10.5099/aj090300274.

[41] R. R. Giraldez and J. L. Zweier, "An improved assay for measurement of nitric oxide synthase activity in biological tissues," *Anal. Biochem.*, vol. 261, no. 1, pp. 29–35, 1998, doi: 10.1006/abio.1998.2721.

[42] D. Tsikas, F. M. Gutzki, and D. O. Stichtenoth, "Circulating and excretory nitrite and nitrate as indicators of nitric oxide synthesis in humans: Methods of analysis," *Eur. J. Clin. Pharmacol.*, vol. 62, no. 1, pp. 51–59, 2006, doi: 10.1007/s00228-005-0020-z.

[43] C. Csonka, T. Páli, P. Bencsik, A. Görbe, P. Ferdinandy, and T. Csont, "Measurement of NO in biological samples," *British Journal of Pharmacology*, vol. 172, no. 6. pp. 1620–1632, 2015, doi: 10.1111/bph.12832.

[44] O. T. Raitakari and D. S. Celermajer, "Flow-mediated dilatation," *Br. J. Clin. Pharmacol.*, vol. 50, no. 5, pp. 397–404, 2000, doi: 10.1046/j.1365-2125.2000.00277.x.

[45] K. E. Sorensen *et al.*, "Non-invasive measurement of human endothelium dependent arterial responses: Accuracy and reproducibility," *Heart*, vol. 74, no. 3, pp. 247–253, 1995, doi: 10.1136/hrt.74.3.247.

[46] D. H. J. Thijssen *et al.*, "The impact of baseline diameter on flow-mediated dilation differs in young and older humans," *Am. J. Physiol. - Hear. Circ. Physiol.*, vol. 295, no. 4, pp. 1594–1598, 2008, doi: 10.1152/ajpheart.00669.2008.

[47] A. Spiers and N. Padmanabhan, "A guide to wire myography.," *Methods Mol. Med.*,

vol. 108, no. 3, pp. 91–104, 2005, doi: 10.1385/1-59259-850-1:091.

[48] O. L. Schjørring, R. Carlsson, and U. Simonsen, "Pressure myography to study the function and structure of isolated small arteries," in *Methods in Molecular Biology*, 2015.

[49] M. Shahid and S. E. Buys, "Assessing murine resistance artery function using pressure myography," *J. Vis. Exp.*, no. 76, pp. 1–7, 2013, doi: 10.3791/50328.

[50] D. Huh, G. A. Hamilton, and D. E. Ingber, "From 3D cell culture to organs-on-chips," *Trends Cell Biol.*, vol. 21, no. 12, pp. 745–754, 2011, doi: 10.1016/j.tcb.2011.09.005.

[51] S. Kim, W. Kim, S. Lim, and J. S. Jeon, "Vasculature-on-a-chip for in vitro disease models," *Bioengineering*, vol. 4, no. 1, 2017, doi: 10.3390/bioengineering4010008.

[52] A. Günther *et al.*, "A microfluidic platform for probing small artery structure and function," *Lab Chip*, vol. 10, no. 18, pp. 2341–2349, 2010, doi: 10.1039/c004675b.

[53] S. Yasotharan, S. Pinto, J. G. Sled, S. S. Bolz, and A. Günther, "Artery-on-a-chip platform for automated, multimodal assessment of cerebral blood vessel structure and function," *Lab Chip*, vol. 15, no. 12, pp. 2660–2669, 2015, doi: 10.1039/c5lc00021a.

[54] B. Dreier, J. Z. Gasiorowski, J. T. Morgan, P. F. Nealey, P. Russell, and C. J. Murphy, "Early responses of vascular endothelial cells to topographic cues," *Am. J. Physiol. - Cell Physiol.*, vol. 305, no. 3, pp. 290–299, 2013, doi: 10.1152/ajpcell.00264.2012.

[55] M. Zhao, H. Bai, E. Wang, J. V. Forrester, and C. D. McCaig, "Electrical stimulation directly induces pre-angiogenic responses in vascular endothelial cells by signaling

through VEGF receptors," *J. Cell Sci.*, vol. 117, no. 3, pp. 397–405, 2004, doi: 10.1242/jcs.00868.

[56] S. F. Kemeny, D. S. Figueroa, A. M. Andrews, K. A. Barbee, and A. M. Clyne, "Glycated collagen alters endothelial cell actin alignment and nitric oxide release in response to fluid shear stress," *J. Biomech.*, vol. 44, no. 10, pp. 1927–1935, 2011, doi: 10.1016/j.jbiomech.2011.04.026.

[57] L. Nivison-Smith and A. S. Weiss, "Alignment of human vascular smooth muscle cells on parallel electrospun synthetic elastin fibers," *J. Biomed. Mater. Res. - Part A*, vol. 100 A, no. 1, pp. 155–161, 2012, doi: 10.1002/jbm.a.33255.

[58] S. Kanno *et al.*, "Establishment of a simple and practical procedure applicable to therapeutic angiogenesis," *Circulation*, vol. 99, no. 20, pp. 2682–2687, 1999, doi: 10.1161/01.CIR.99.20.2682.

[59] R. Steward, D. Tambe, C. Corey Hardin, R. Krishnan, and J. J. Fredberg, "Fluid shear, intercellular stress, and endothelial cell alignment," *Am. J. Physiol. - Cell Physiol.*, vol. 308, no. 8, pp. 657–664, 2015, doi: 10.1152/ajpcell.00363.2014.

[60] J. Feng, M. B. Chan-Park, J. Shen, and V. Chan, "Quick layer-by-layer assembly of aligned multilayers of vascular smooth muscle cells in deep microchannels," *Tissue Eng.*, vol. 13, no. 5, pp. 1003–1012, 2007, doi: 10.1089/ten.2006.0223.

[61] O. Wichterle and D. Lím, "Hydrophilic Gels for Biological Use," *Nature*, 1960, doi: 10.1038/185117a0.

[62] E. M. Ahmed, "Hydrogel: Preparation, characterization, and applications: A review," *J. Adv. Res.*, vol. 6, no. 2, pp. 105–121, 2015, doi: 10.1016/j.jare.2013.07.006.

[63]   S. Khorshidi and A. Karkhaneh, "Hydrogel/fiber conductive scaffold for bone tissue engineering," *J. Biomed. Mater. Res. - Part A*, 2018, doi: 10.1002/jbm.a.36282.

[64]   M. Foox and M. Zilberman, "Drug delivery from gelatin-based systems," *Expert Opinion on Drug Delivery*. 2015, doi: 10.1517/17425247.2015.1037272.

[65]   N. C. Cheng, W. J. Lin, T. Y. Ling, and T. H. Young, "Sustained release of adipose-derived stem cells by thermosensitive chitosan/gelatin hydrogel for therapeutic angiogenesis," *Acta Biomater.*, 2017, doi: 10.1016/j.actbio.2017.01.060.

[66]   P. P. Partyka *et al.*, "Mechanical stress regulates transport in a compliant 3D model of the blood-brain barrier," *Biomaterials*, vol. 115, pp. 30–39, 2017, doi: 10.1016/j.biomaterials.2016.11.012.

[67]   S. Young, M. Wong, Y. Tabata, and A. G. Mikos, "Gelatin as a delivery vehicle for the controlled release of bioactive molecules," *J. Control. Release*, vol. 109, no. 1–3, pp. 256–274, 2005, doi: 10.1016/j.jconrel.2005.09.023.

[68]   M. Sun, X. Sun, Z. Wang, S. Guo, G. Yu, and H. Yang, "Synthesis and properties of gelatin methacryloyl (GelMA) hydrogels and their recent applications in load-bearing tissue," *Polymers (Basel).*, vol. 10, no. 11, 2018, doi: 10.3390/POLYM10111290.

[69]   H. Qi, Y. Du, L. Wang, H. Kaji, H. Bae, and A. Khademhosseini, "Patterned differentiation of individual embryoid bodies in spatially organized 3D hybrid microgels," *Adv. Mater.*, 2010, doi: 10.1002/adma.201002873.

[70]   I. Noshadi *et al.*, "In vitro and in vivo analysis of visible light crosslinkable gelatin methacryloyl (GelMA) hydrogels," *Biomater. Sci.*, 2017, doi: 10.1039/c7bm00110j.

[71]   L. Gitlin, P. Schulze, S. Ohla, H. J. Bongard, and D. Belder, "Surface modification

of PDMS microfluidic devices by controlled sulfuric acid treatment and the application in chip electrophoresis," *Electrophoresis*, vol. 36, no. 3, pp. 449–456, 2015, doi: 10.1002/elps.201400269.

[72]   H. D. Intengan and E. L. Schiffrin, "Structure and mechanical properties of resistance arteries in hypertension: Role of adhesion molecules and extracellular matrix determinants," *Hypertension*, vol. 36, no. 3, pp. 312–318, 2000, doi: 10.1161/01.HYP.36.3.312.

[73]   H. E. Abaci, Y. I. Shen, S. Tan, and S. Gerecht, "Recapitulating physiological and pathological shear stress and oxygen to model vasculature in health and disease," *Sci. Rep.*, vol. 4, pp. 1–9, 2014, doi: 10.1038/srep04951.

[74]   K. M. Chrobak, D. R. Potter, and J. Tien, "Formation of perfused, functional microvascular tubes in vitro," *Microvasc. Res.*, vol. 71, no. 3, pp. 185–196, 2006, doi: 10.1016/j.mvr.2006.02.005.

[75]   C. Bertulli *et al.*, "Image-Assisted Microvessel-on-a-Chip Platform for Studying Cancer Cell Transendothelial Migration Dynamics," *Sci. Rep.*, vol. 8, no. 1, pp. 1–14, 2018, doi: 10.1038/s41598-018-30776-0.

[76]   C. C. Lee *et al.*, "Multistep synthesis of a radiolabeled imaging probe using integrated microfluidics," *Science (80-.).*, vol. 310, no. 5755, pp. 1793–1796, 2005, doi: 10.1126/science.1118919.

[77]   R. Seghir and S. Arscott, "Extended PDMS stiffness range for flexible systems," *Sensors Actuators, A Phys.*, vol. 230, pp. 33–39, 2015, doi: 10.1016/j.sna.2015.04.011.

[78]   H. Stratesteffen, M. Köpf, F. Kreimendahl, A. Blaeser, S. Jockenhoevel, and H.

Fischer, "GelMA-collagen blends enable drop-on-demand 3D printablility and promote angiogenesis," *Biofabrication*, 2017, doi: 10.1088/1758-5090/aa857c.

[79] I. Pepelanova, K. Kruppa, T. Scheper, and A. Lavrentieva, "Gelatin-methacryloyl (GelMA) hydrogels with defined degree of functionalization as a versatile toolkit for 3D cell culture and extrusion bioprinting," *Bioengineering*, vol. 5, no. 3, 2018, doi: 10.3390/bioengineering5030055.

[80] I. Xanthis *et al.*, "B1 Integrin Is a Sensor of Blood Flow Direction," *J. Cell Sci.*, vol. 132, no. 11, 2019, doi: 10.1242/JCS.229542.

[81] Y. Li *et al.*, "Engineering cell alignment in vitro," *Biotechnol. Adv.*, vol. 32, no. 2, pp. 347–365, 2014, doi: 10.1016/j.biotechadv.2013.11.007.

[82] D. H. Kim *et al.*, "Nanoscale cues regulate the structure and function of macroscopic cardiac tissue constructs," *Proc. Natl. Acad. Sci. U. S. A.*, vol. 107, no. 2, pp. 565–570, 2010, doi: 10.1073/pnas.0906504107.

[83] J. S. Choi, Y. Piao, and T. S. Seo, "Circumferential alignment of vascular smooth muscle cells in a circular microfluidic channel," *Biomaterials*, vol. 35, no. 1, pp. 63–70, 2014, doi: 10.1016/j.biomaterials.2013.09.106.

[84] G. M. Fomovsky and J. W. Holmes, "Evolution of scar structure, mechanics, and ventricular function after myocardial infarction in the rat," *Am. J. Physiol. - Hear. Circ. Physiol.*, vol. 298, no. 1, pp. 221–228, 2010, doi: 10.1152/ajpheart.00495.2009.

[85] W. J. Karlon, J. W. Covell, A. D. Mcculloch, J. J. Hunter, and J. H. Omens, "Automated measurement of myofiber disarray in transgenic mice with ventricular expression of ras," *Anat. Rec.*, vol. 252, no. 4, pp. 612–625, 1998, doi: